

Variational Bayesian Learning Based Localization and Channel Reconstruction in RIS-aided Systems

Yunfei Li, Yiting Luo, Xianda Wu, Zheng Shi, Shaodan Ma and Guanghua Yang

Abstract—The emerging immersive and autonomous services have posed stringent requirements on both communications and localization. By considering the great potential of reconfigurable intelligent surface (RIS), this paper focuses on the joint channel estimation and localization for RIS-aided wireless systems. As opposed to existing works that treat channel estimation and localization independently, this paper exploits the intrinsic coupling and nonlinear relationships between the channel parameters and user location for enhancement of both localization and channel reconstruction. By noticing the non-convex, nonlinear objective function and the sparser angle pattern, a variational Bayesian learning-based framework is developed to jointly estimate the channel parameters and user location through leveraging an effective approximation of the posterior distribution. The proposed framework is capable of unifying near-field and far-field scenarios owing to exploitation of sparsity of the angular domain. Since the joint channel and location estimation problem has a closed-form solution in each iteration, our proposed iterative algorithm performs better than the conventional particle swarm optimization (PSO) and maximum likelihood (ML) based ones in terms of computational complexity. Simulations demonstrate that the proposed algorithm almost reaches the Bayesian Cramer-Rao bound (BCRB) and achieves a superior estimation accuracy by comparing to the PSO and the ML algorithms.

Index Terms—BCRB, channel estimation, localization, reconfigurable intelligent surface, and variational Bayesian.

I. INTRODUCTION

A. Motivation and Literature Review

The wireless communications is undergoing a significant transformation, marked by increased demands for wireless resources and adaptive intelligence. This shift is driven by the growing need for high-quality service and precise localization accuracy. Sectors like autonomous driving, smart transportation, and unmanned aerial vehicles (UAVs) exemplify this change, relying on attributes such as high data rates, unwavering reliability, and precise positioning. Meeting these demands requires the cultivation of innovative techniques to not only achieve precise localization but also facilitate high-speed communications. For instance, recent studies highlight the emergence of large antenna arrays as a transformative technology. In [1], Bayesian channel estimation techniques tailored for multi-user massive multiple input multiple output (MIMO) systems with extensive antenna arrays are explored.

[2] introduces an innovative methodology for direction-of-arrival (DoA) estimation designed specifically for large antenna arrays, leveraging hybrid analog and digital architectures. This approach opens new avenues for optimizing spatial awareness in communication systems. Additionally, [3] delves into communication and localization using extremely large lens antenna arrays. Besides, another promising technique is the use of reconfigurable intelligent surfaces (RIS), capable of altering the physical propagation environment to amalgamate signals at the receiver either destructively or constructively. The literature extensively reports on the applications of RIS in localization and communications.

The RIS is composed of numerous reflecting elements capable of actively modifying the phases and amplitudes of incident electromagnetic waves through a smart microcontroller, as highlighted in [4]. The cost-effectiveness of RIS hardware allows for its widespread use, providing additional controllable communication paths that enhance system performance in terms of reliability, energy/spectrum efficiency, and security, as discussed in [5–8]. Consequently, RIS technology holds the promise of significantly improving wireless communications and localization, especially in the context of beyond fifth generation (B5G) or sixth generation (6G) communications, as emphasized in [9, 10]. A substantial body of research has been dedicated to exploring and harnessing the benefits and potentials of RIS-aided communications, reflecting the growing interest and recognition of its transformative impact [11, 12]. In recent literatures, a Bayesian framework was proposed in [13] for user localization and tracking in RIS-aided MIMO systems. Delving into statistical methods for enhanced channel estimation accuracy, this work establishes a foundation for robust communication systems. Equally pivotal is the exploration in [14], who delve into RIS-assisted multi-user multiple input single output (MISO) communications, emphasizing the exploitation of statistical channel state information (CSI) to optimize system performance. This article also draws insights from the study conducted in [15] on multi-hop RIS-empowered terahertz communications, presenting a novel deep reinforcement learning based hybrid beamforming design and showcasing the versatility of RIS in the Terahertz frequency range. The comprehensive framework proposed in [16] for channel estimation with RIS, further establishes the general applicability of RIS across diverse communication scenarios. Insights into robust channel estimation for RIS-aided millimeter-wave systems, addressing challenges such as RIS blockage, are contributed in [17]. Additionally, [18] provides valuable perspectives on RIS-aided wireless communications, covering prototyping, adaptive beamforming, and real-world field trials.

However, most of the prior works frequently assumed either perfect CSI or precise user location for RIS-aided systems

Y. Li and Y. Luo are with the Department of Electrical Engineering, Anhui Polytechnic University, Wuhu City, China (email: lyf@mail.ahpu.edu.cn; lyt1222@ahpu.edu.cn).

X. Wu is with the School of Electronics and Information Engineering, South China Normal University, Foshan 528000, China (email: xian-dawu@m.scnu.edu.cn).

G. Yang and Z. Shi are with the School of Intelligent Systems Science and Engineering, Jinan University, Zhuhai 519070, China (e-mails: zheng-shi@jnu.edu.cn; ghyang@jnu.edu.cn).

S. Ma is with the State Key Laboratory of Internet of Things for Smart City and the Department of Electrical and Computer Engineering, University of Macau, Taipa, Macao, China (e-mail: shaodanma@um.edu.mo).

that are obviously too optimistic for practical applications. To address this issue, there exist a few works that are concerned with the imperfect CSI and inaccurate localization in RIS-aided systems. In what follows, the channel estimation and the user localization in RIS-aided systems are individually investigated.

With regard to the channel estimation of RIS-aided systems, the channels can be divided into far-field and near-field scenarios, as evidenced by recent studies. [19] presents a pioneering study, introducing a hybrid far- and near-field modeling approach for reconfigurable intelligent surface (RIS) assisted Vehicle-to-Vehicle (V2V) channels. Their sub-array partition-based methodology emphasizes the intricate interplay between far-field and near-field effects, offering valuable insights for optimizing communication scenarios in V2V channels. [20] provides a comprehensive exploration of near-field MIMO communications in the context of 6G evolution. [21] contributes to the field by focusing on RIS-aided near-field localization and channel estimation within the terahertz frequency range, which offers valuable insights for terahertz communication systems. [22] explores near-field tracking with large antenna arrays, discussing fundamental limits and practical algorithms and contributes essential knowledge on the challenges and potential solutions associated with large antenna arrays in the context of near-field tracking applications. Furthermore, channel estimation methods in the RIS-aided systems can be broadly categorized into parametric estimation methods and statistical estimation methods. In the domain of parametric channel estimation, various approaches address the sparsity or low-rank characteristics of RIS-aided system channels. Noteworthy works include [23–28], where methods such as message-passing algorithms, double-structured orthogonal matching pursuit (DS-OMP), and two-stage algorithms are proposed to estimate RIS-aided system channels while considering their inherent sparsity or low-rank properties. Additionally, works like [23, 27, 29] present techniques involving alternating least squares, variational approximate message passing, atomic norm minimization, and wideband modeling to address RIS-aided channel estimation challenges. On the statistical front, similar efforts have been made to exploit RIS-aided communication systems. Examples include [30], which estimates the instantaneous CSI of a single-user RIS-aided system using a hierarchical training reflection matrix design algorithm. In [31], research delves into joint data detection and channel estimation for hybrid Reconfigurable Intelligent Surface (HRIS)-aided millimeter-wave orthogonal time-frequency space (OTFS) systems. Additionally, [32] considers imperfect channel state information and correlated Rayleigh fading channels in the context of RIS-assisted multiple input single output (MISO) systems with hardware impairments. These statistical channel estimation approaches encompass a range of scenarios, offering insights into addressing challenges related to imperfect information and hardware impairments in RIS-assisted communication systems.

On the other hand, localization remains a critical concern in RIS-aided communication systems, with several studies shedding light on diverse aspects of this intricate challenge. Notably, [33] reported on far-field localization in both the

uplink and downlink of RIS-aided systems. Further exploration in [34] delved into indoor far-field localization scenarios, deriving the CRLB in closed-form and showcasing the RIS as a fundamental technique for achieving high indoor localization accuracy. [35] analyzed the RIS-aided localization error bound, demonstrating superior performance compared to systems without RIS assistance. While some works, such as [36] and [37], focused on localization algorithms for RIS-aided systems, channel estimation was neglected. Addressing this gap, Keykhosravi et al. [38] solved the synchronization and localization problem for RIS-aided single input single output (SISO) systems, assuming perfect CSI. They utilized maximum likelihood (ML) estimation by leveraging the dominance of the direct link signal power over the reflected signal power. ML-based estimation approaches were also proposed in [39], accompanied by the derivation of corresponding CRLB. Moreover, RIS-aided localization challenges were explored in B5G [40] and mm-Wave MIMO systems [41]. Despite these endeavors, the localization of RIS-aided systems remains in its infancy, with numerous associated problems yet to be explored.

The majority of the aforementioned research works have predominantly concentrated on addressing either the channel estimation or localization challenges in the RIS-assisted communications. However, the intricacies arise as the joint estimation of channel states and localization becomes paramountly important, given the inherent coupling of user locations and channel estimation problems, which is a consequence of the shared environmental dependencies on channel gains, delays, and angles, significantly intensifying the complexity of the estimation problem. In a notable attempt to tackle this challenge, [42] proposed a solution assuming a twin-RIS structure to facilitate channel estimation through tensor decomposition. The estimated CSI was then leveraged for the localization of far-field users. Similarly, in [43], researchers delved into the intricacies of near-field joint localization and channel estimation, specifically in an extremely large RIS-aided MIMO system. Regrettably, these approaches were formulated under the assumption of specialized RIS structures, rendering them inapplicable to more general scenarios. The quest for effective methodologies that can accommodate diverse RIS configurations remains a pressing challenge in advancing the joint estimation of channel states and localization in RIS-assisted communications.

B. Our Contributions

In this paper, we dig into the complicated joint channel estimation and localization for RIS-aided wireless systems, focusing on a more general RIS-aided configuration. In this paper, the transmitter possesses only partial prior statistical knowledge regarding the user's location, channel gains, and the angle of departure (AoD). The challenge lies in the intricate interplay among the user's location, nonlinear phase shifts, channel gains, and AoD terms, rendering the joint estimation problem highly intricate. To address this complexity, a variational Bayesian framework [44, 45], which is also applied to the user detection and channel estimation [46], vehicle to

vehicle channel estimation [47], signal recovery[48], will be developed by capitalizing on the sparser angle pattern and the prior channel information. In summary, the contributions of this paper are outlined as follows.

- Unlike [43] and [42] that take into account the twin-RIS structure and extra large RIS requirements, a joint localization and channel estimation problem is considered for a general RIS-aided communication system with fewer constraints on the RIS structures.
- The sparser angle pattern and the prior channel information motivate us to develop a variational Bayesian learning-based framework of joint channel and location estimation. The proposed algorithm is applicable to both near-field but also far-field scenarios owing to the exploitation of the sparsity of the angular domain.
- The complexity analysis of the proposed algorithm is conducted in this paper. Since the joint channel and location estimation problem has a closed-form solution in each iteration, the proposed iterative algorithm converges faster than the PSO and ML-based ones.
- The BCRB of the joint estimation problem is derived to show the performance bounds of the joint estimation problem. Monte Carlo simulations demonstrate that the proposed algorithm almost reaches the Bayesian Cramer-Rao bound (BCRB).

C. Organization

The remainder of this paper is organized as follows. In Section II, the problem of joint channel estimation and localization in RIS-aided systems is formulated. A variational Bayesian learning-based joint channel and location estimation algorithm is proposed in Section III. Section IV carries out the complexity analysis of the proposed algorithm. Finally, the simulation results are presented in Section V and the paper is concluded in Section VI.

II. SYSTEM MODEL

We consider a RIS-aided system with an access point (AP) equipped with a single antenna and single antenna user in Fig.1. The RIS is deployed for the aid of reflecting the signals from the AP to the user. The position of the AP is $\mathbf{p}_a = [x_a, y_a, z_a]^T$ and the position of the user is $\mathbf{p}_u = [x_u, y_u, z_u]^T$. We assume that the RIS is a uniform planar array with $M \times N$ reflecting elements. In the RIS, the inter-element distance between the column elements and the row elements are equal to d . The origin coordinate of the RIS is given by $\mathbf{p}_r = [x_r, y_r, z_r]^T$. The (m, n) -th element is located at $\mathbf{p}_r^{m,n} = [x_r + (m-1)d, y_r, z_r + (n-1)d]^T$. The user receives L OFDM subcarriers both from the AP directly and from the RIS. Similar to [?], we assume the reflected paths always exist and the reflected signals are received by

the user for localization and channel estimation. Hence, the received signal at the user side is given by [38, 49, 50],

$$\mathbf{r}_t = \underbrace{\alpha_{au} \sqrt{P_w} \varphi(\zeta_{au})}_{\Xi_{au}^t} + \underbrace{\alpha_{ru} \sqrt{P_w} \varphi(\zeta_{ru}) \mathbf{a}^T(\theta, \vartheta) \text{diag}(\boldsymbol{\Omega}_t) \mathbf{a}(\psi, \phi)}_{\Xi_{ru}^t} + \varepsilon_t, \quad (1)$$

where ε_t is the zero-mean Gaussian noise with variance matrix $\delta \mathbf{I}$. α_{au} is the unknown complex channel gain of the AP-user link and α_{ru} is assumed to be an unknown complex channel gain of the AP-RIS-user link due to the random reflection in RIS. $\sqrt{P_w}$ is the transmitted pilot symbol. $\boldsymbol{\omega}_t = \text{vec}(\boldsymbol{\Lambda}_t) \in \mathbb{C}^{MN \times 1}$ with the known phase shifts of the RIS elements at t -th transmission is given by $\boldsymbol{\Lambda}_t \in \mathbb{C}^{M \times N}$ and $\boldsymbol{\Omega}_t = \text{diag}(\boldsymbol{\omega}_t)$. ζ_{au} and ζ_{ru} are the delays of the AP-user link and the AP-RIS-user link respectively and respectively are given by

$$\zeta_{au} = \frac{\|\mathbf{p}_a - \mathbf{p}_u\|_2}{c}, \quad (2)$$

and

$$\zeta_{ru} = \frac{\|\mathbf{p}_a - \mathbf{p}_r\|_2 + \|\mathbf{p}_r - \mathbf{p}_u\|_2}{c}, \quad (3)$$

and the phase shifts caused by the delays are given by $\varphi(\zeta_{au}) = [1, e^{-j2\pi\zeta_{au}\Delta f}, \dots, e^{-j2\pi(L-1)\zeta_{au}\Delta f}]^T$ and $\varphi(\zeta_{ru}) = [1, e^{-j2\pi\zeta_{ru}\Delta f}, \dots, e^{-j2\pi(L-1)\zeta_{ru}\Delta f}]^T$ respectively. Δf is the frequency spacing. In (1), the steering vector $\mathbf{a}(\theta, \vartheta) \in \mathbb{C}^{MN \times 1}$ is given by

$$\mathbf{a}(\theta, \vartheta) = \mathbf{a}_r(\theta, \vartheta) \otimes \mathbf{a}_c(\theta, \vartheta), \quad (4)$$

where \otimes is the Kronecker product and θ, ϑ are the azimuth and elevation angles from the AP to the RIS and these angles are assumed to be known. The $\mathbf{a}_r(\theta, \vartheta)$ and $\mathbf{a}_c(\theta, \vartheta)$ are respectively given by

$$\mathbf{a}_r(\theta, \vartheta) = [1, e^{j\tau}, \dots, e^{j(M-1)\tau}]^T, \quad (5)$$

and

$$\mathbf{a}_c(\theta, \vartheta) = [1, e^{j\nu}, \dots, e^{j(N-1)\nu}]^T, \quad (6)$$

where $\tau = \frac{2\pi d}{\lambda} \cos \vartheta$ and $\nu = \frac{2\pi d}{\lambda} \cos \theta \sin \vartheta$.

Similarly $\mathbf{a}(\psi, \phi) \in \mathbb{C}^{MN \times 1}$ can be given by

$$\mathbf{a}(\psi, \phi) = \mathbf{a}_r(\psi, \phi) \otimes \mathbf{a}_c(\psi, \phi). \quad (7)$$

with

$$\mathbf{a}_r(\psi, \phi) = [1, e^{jv}, \dots, e^{j(M-1)v}]^T, \quad (8)$$

and

$$\mathbf{a}_c(\psi, \phi) = [1, e^{j\kappa}, \dots, e^{j(N-1)\kappa}]^T. \quad (9)$$

where $v = \frac{2\pi d}{\lambda} \cos \psi$ and $\kappa = \frac{2\pi d}{\lambda} \cos \psi \sin \phi$ for the far-field scenarios and

$$\mathbf{a}(\psi, \phi) = \exp \left\{ j \frac{2\pi}{\lambda} \left[\mathbf{F}^T \mathbf{p}_r^{m,n} - \frac{1}{2d_{m,n}} \tilde{\mathbf{F}}^T \tilde{\mathbf{p}}_r^{m,n} \right] \right\}, \quad (10)$$

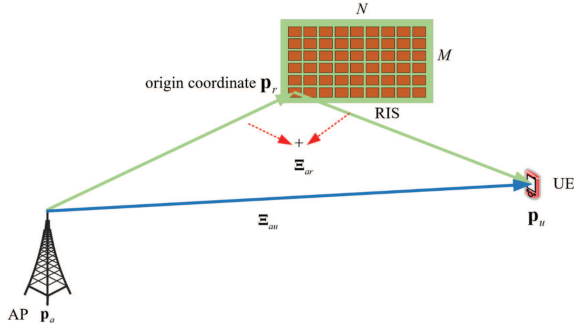


Fig. 1: The system model

for the near-field scenarios¹ and $d_{m,n}$ is the distance between the (m,n) -th element and the origin coordinate of RIS. $\tilde{\mathbf{p}}_r^{m,n} = [\mathbf{p}_r^{m,n} - \mathbf{p}_r]^2$ and $[\cdot]^2$ represents the element-wise square. $\mathbf{F} = [\cos \phi \sin \psi, \sin \phi \sin \psi, \cos \psi]$ and $\tilde{\mathbf{F}} = [1 - \cos^2 \phi \sin^2 \psi, 1 - \sin^2 \phi \sin^2 \psi, \sin^2 \psi]$. The angles ϕ and ψ are assumed to be unknown in both scenarios.

By collecting the T snapshots of the received signal $\mathbf{R} = [\mathbf{r}_1, \dots, \mathbf{r}_T]$, the system model can be given by

$$\mathbf{R} = \underbrace{\alpha_{au} \sqrt{P_w} \boldsymbol{\varphi}(\zeta_{au}) \mathbf{1}^T}_{\boldsymbol{\Xi}_{au}} + \underbrace{\alpha_{ru} \sqrt{P_w} \boldsymbol{\varphi}(\zeta_{ru}) (\boldsymbol{\Upsilon} \mathbf{a}(\psi, \phi))^T}_{\boldsymbol{\Xi}_{ru}} + \boldsymbol{\varepsilon}, \quad (11)$$

where $\boldsymbol{\Upsilon} = [\boldsymbol{\Upsilon}_1^T, \dots, \boldsymbol{\Upsilon}_T^T]^T$ and $\boldsymbol{\Upsilon}_t = \mathbf{a}^T(\theta, \vartheta) \text{diag}(\boldsymbol{\Omega}_t)$. The likelihood function can be given by

$$p(\mathbf{R}|\boldsymbol{\Theta}) = \prod_t p(\mathbf{r}(t)|\boldsymbol{\Theta}) \\ \propto \prod_{t=1}^T \exp\left(-\frac{1}{2\delta} (\mathbf{r}_t - \boldsymbol{\Xi}_{au}^t - \boldsymbol{\Xi}_{ru}^t)^H (\mathbf{r}_t - \boldsymbol{\Xi}_{au}^t - \boldsymbol{\Xi}_{ru}^t)\right), \quad (12)$$

where $\boldsymbol{\Theta} = [\boldsymbol{\varphi}^T(\zeta_{au}), \boldsymbol{\varphi}^T(\zeta_{ru}), \psi, \phi, \alpha_{au}, \alpha_{ru}]$. In the paper, we focus on the estimation of the user location and channel state information with the aid of the RIS. In (12), the direct maximization is intractable due to two extremely challenging problems: the coupling unknown parameter and the nonlinear steering vector $\mathbf{a}(\psi, \phi)$. To obtain the solution of the user location and CSI, we proposed a variational Bayesian inference-based estimation algorithm.

III. VARIATIONAL BAYESIAN LEARNING-BASED LOCALIZATION AND CHANNEL ESTIMATION ALGORITHM

A. Sparse Representation

Considering the sparsity of the angles in $\mathbf{a}(\psi, \phi)$, the system model in (7) is reformulated via sparse representation. First, the angle spread of ψ, ϕ are both assumed to be $[-\frac{\pi}{2}, \frac{\pi}{2}]$

¹It means the RIS and the user are in far-field or near-field scenarios. The steering vector for near field scenarios is an approximation to the exact one according to [51]. For channels encompassing mixed near and far-field components, we extend the system model to accommodate multiple users, as outlined in [52]. However, it's worth noting that the multiple users scenario necessitates the phase optimization of RIS elements, a task that exceeds the feasibility scope of the proposed algorithm.

and the spread can be both equally divided into P and Q resolutions respectively, then we can obtain

$$\boldsymbol{\Gamma} = \begin{bmatrix} (\bar{\psi}_1, \bar{\phi}_1) & \cdots & (\bar{\psi}_1, \bar{\phi}_Q) \\ \vdots & & \vdots \\ (\bar{\psi}_P, \bar{\phi}_1) & \cdots & (\bar{\psi}_P, \bar{\phi}_Q) \end{bmatrix} \in \mathbb{C}^{P \times Q}. \quad (13)$$

Using the vectorization of (13), it yields

$$\bar{\boldsymbol{\theta}} = [(\bar{\psi}_1, \bar{\phi}_1) \cdots (\bar{\psi}_1, \bar{\phi}_Q) \cdots (\bar{\psi}_P, \bar{\phi}_Q)] \in \mathbb{C}^{1 \times PQ}. \quad (14)$$

Embedding (14) into (7), we can obtain

$$\bar{\mathbf{A}} = \mathbf{a}(\bar{\boldsymbol{\theta}}) = [\mathbf{a}(\bar{\psi}_1, \bar{\phi}_1) \cdots \mathbf{a}(\bar{\psi}_P, \bar{\phi}_Q)] \in \mathbb{C}^{MN \times PQ}. \quad (15)$$

Though the true angles are continuous variables and may not fall on the grid points, the off-grid errors can be ignorable given enough resolutions of P and Q . Hence, we apply the on-grid model and the steering vector is given by

$$\mathbf{A} = [\mathbf{a}(\bar{\psi}_1, \bar{\phi}_1) \cdots \mathbf{a}(\bar{\psi}_p, \bar{\phi}_q), \cdots \mathbf{a}(\bar{\psi}_P, \bar{\phi}_Q)] \\ \in \mathbb{C}^{MN \times PQ}. \quad (16)$$

Therefore, the reflected link $\boldsymbol{\Xi}_{ru}^t$ can be reformulated as

$$\boldsymbol{\Xi}_{ru}^t = \sqrt{P_w} \boldsymbol{\varphi}(\zeta_{ru}) \boldsymbol{\Upsilon}_t \mathbf{A} \boldsymbol{\Delta}_{ru}, \quad (17)$$

where $\boldsymbol{\Delta}_{ru} \in \mathbb{C}^{PQ \times 1}$ is a vector with only one unknown nonzero element α_{ru} at unknown location of $\boldsymbol{\Delta}_{ru}$. The system model can be approximated as

$$\mathbf{R} = \underbrace{\alpha_{au} \sqrt{P_w} \boldsymbol{\varphi}(\zeta_{au}) \mathbf{1}^T}_{\boldsymbol{\Xi}_{au}} + \underbrace{\sqrt{P_w} \boldsymbol{\varphi}(\zeta_{ru}) (\boldsymbol{\Upsilon} \mathbf{A} \boldsymbol{\Delta}_{ru})^T}_{\boldsymbol{\Xi}_{ru}} + \boldsymbol{\varepsilon}, \quad (18)$$

where $\mathbf{1} \in \mathbb{R}^{T \times 1}$ is a column vector and $\boldsymbol{\varepsilon} = [\varepsilon_1^T, \dots, \varepsilon_T^T]^T$. Hence, the likelihood function of (18) can be given by

$$p(\mathbf{R}|\boldsymbol{\nu}) \\ \propto \exp\left(-(\mathbf{R} - \boldsymbol{\Xi}_{au} - \boldsymbol{\Xi}_{ru})^H \boldsymbol{\Sigma}^{-1} (\mathbf{R} - \boldsymbol{\Xi}_{au} - \boldsymbol{\Xi}_{ru})\right), \quad (19)$$

where $\boldsymbol{\nu} = [\boldsymbol{\varphi}^T(\zeta_{au}), \boldsymbol{\varphi}^T(\zeta_{ru}), \psi, \phi, \alpha_{au}, \boldsymbol{\Delta}_{ru}]$ and $\boldsymbol{\Sigma}$ is the diagonal covariance matrix with all diagonal elements δ .

The UE location estimation is via the maximum likelihood estimation in (19) and the main objective is to estimate the parameters $\phi, \psi, \zeta_{au}, \zeta_{ru}$. For the angles ψ, ϕ , they are represented sparsely in (17) and it is equivalent to estimate the nonzero elements variable in the sparse vector $\boldsymbol{\Delta}_{ru}$. For the delays ζ_{au} and ζ_{ru} , it is intractable to acquire the closed-form solution via direct maximization of (19). Considering the estimation of unknown parameters via maximum a posterior (MAP), the prior distributions of the unknown parameters require further clarifications:

- The line-of-sight complex channel gain α_{au} is assumed to subject to a complex Gaussian distribution as

$$p(\alpha_{au}) = \mathcal{CN}(\alpha_{au} | \mu_{\alpha_{au}}, \delta_{\alpha_{au}}). \quad (20)$$

- In the paper, the line-of-sight time delay ζ_{au} and the reflecting path time delay ζ_{ru} are nonlinear to the likelihood function (12) and it is difficult to find the closed-form estimation to the time delays. Hence, we turn to estimate

the two phase shifts $\varphi(\zeta_{au})$ and $\varphi(\zeta_{ru})$. However, it is challenging to obtain the precise prior distributions of the phase shift variables. Hence, we assume the non-informative complex Gaussian distributions

$$p(\Psi_i) = \mathcal{CN}(\Psi_i | \mu_{\Psi_i}, \Sigma_{\Psi_i}), \quad (21)$$

with $\delta_{\Psi_i} \rightarrow \infty$ and $\Psi_i \in [\varphi(\zeta_{au}), \varphi(\zeta_{ru})]$. In practice, the variance can be replaced by relatively large positive values.

- For the sparse representation parameter Δ_{ru} , only one nonzero element exists at an unknown location and the other elements are zeros. The nonzero element is also unknown. Therefore, it is assumed that each element Δ_{ru}^i in the sparse vector Δ_{ru} follows a mixture Gaussian distribution [53] as follows

$$p(\Delta_{ru}) = \prod_{i=1}^{\text{PQ}} p(\Delta_{ru}^i) = \prod_{i=1}^{\text{PQ}} \prod_{l=1}^2 \mathcal{CN}(\Delta_{ru}^i | \mu_{\Delta}^l, w_{\Delta}^{-1})^{g_{i,l}}, \quad (22)$$

where complex Gaussian distribution with $\mu_{\Delta}^1 = 0$ and $w_{\Delta}^{-1} \gg \mu_{\Delta}^1$ is to enforce a prior distribution to the zero elements. $\mathbf{g}_i = [g_{i,1}, g_{i,2}]$ is indicator vector and is given by

$$\mathbf{g}_i = \begin{cases} (1, 0) & \Delta_{ru}^i \neq 0, \\ (0, 1) & \Delta_{ru}^i = 0. \end{cases} \quad (23)$$

- The inverse variance w_{Δ}^i in (22) is further constrained by imposing a prior distribution and we assume a inverse variance w_{Δ}^i , which is given by

$$p(w_{\Delta}) = \prod_{i=1}^{\text{PQ}} p(w_{\Delta}^i) = \prod_{i=1}^{\text{PQ}} \Gamma(w_{\Delta}^i | a_i, b_i), \quad (24)$$

where $\Gamma(\cdot)$ is the Gamma distribution and a_i, b_i are the known parameters of the Gamma distribution and $w_{\Delta} = [w_{\Delta}^1, \dots, w_{\Delta}^{\text{PQ}}]$.

- Therefore, the indicator variable \mathbf{g}_i can be modeled to follow a non-informative categorical distribution, which is given by

$$p(\mathbf{r} | \chi) = \prod_{i=1}^{\text{PQ}} \prod_{l=1}^2 p(g_{i,l} | \chi_l) = \prod_{i=1}^{\text{PQ}} \prod_{l=1}^2 \chi_l^{g_{i,l}}, \quad (25)$$

with $\mathbf{g} = [\mathbf{g}_1, \dots, \mathbf{g}_{\text{PQ}}]$ and $\chi = [\chi_1, \chi_2] = \left[\frac{1}{\text{PQ}}, 1 - \frac{1}{\text{PQ}} \right]$. For easy presentation, we denote an unknown variable vector $\mathcal{W} = [\varphi^T(\zeta_{au}), \varphi^T(\zeta_{ru}), \psi, \phi, \Delta_{ru}, \mathbf{g}, w_{\Delta}]$.

B. Variational Bayesian Learning Framework

Based on the problem reformulation, our goal is to learn the true posterior distribution of the channel parameters and locations. Then the delay parameters, the online angles and the channel gains can be estimated as a maximum posterior problem as follows

$$\hat{\mathcal{W}} = \operatorname{argmax} \int p(\mathbf{R} | \mathcal{W}) p(\mathcal{W}) d\mathbf{g} dw_{\Delta}, \quad (26)$$

where involves numerous prior distributions, multiple integrals, coupled channel and location parameters, and the non-linear non-convex objective function. Thus it is intractable to directly obtain learning features and find a closed-form solution. Hence, we focus on finding an approximation distribution to the true posterior distribution, which is also tractable for the MAP or MMSE estimators.

In the variational Bayesian learning framework, we aim at finding a variational $q(\mathcal{W})$ to the posterior distribution $p(\mathcal{W} | \mathbf{R})$ in (26) and the variational distribution $q(\mathcal{W})$ is tractable. Revoked by the mean-field theory and assumption, we factorize the variational distribution $q(\mathcal{W})$ as

$$q(\mathcal{W}) = \prod_{\mathcal{W}_k \in \mathcal{W}} q(\mathcal{W}_k), \quad (27)$$

To measure the approximation between the variational distribution $q(\mathcal{W})$ and the true distribution $p(\mathcal{W} | \mathbf{R})$, Kullback-Leibler (KL) divergence [54] is introduced and minimized as

$$\text{KL}(q(\mathcal{W}) || p(\mathcal{W} | \mathbf{R})) = -\mathbb{E}_{q(\mathcal{W})} \left\{ \ln \frac{p(\mathcal{W} | \mathbf{R})}{q(\mathcal{W})} \right\} \geq 0, \quad (28)$$

where $\mathbb{E}_{q(\mathcal{W})}$ is the expectation with respect to $q(\mathcal{W})$ and the equality holds only when $q(\mathcal{W}) = p(\mathcal{W} | \mathbf{R})$. Based on the mean-field theory in (27) and the alternative optimization method, the variational distribution can be iteratively approximated as [55]

$$q^{(\xi)}(\mathcal{W}_k) \propto \exp \left\{ \mathbb{E}_{q^{(\xi)}(\mathcal{W}_{\setminus k})} [\ln p(\mathcal{W}, \mathbf{R})] \right\}, \quad (29)$$

where $q^{(\xi)}(\mathcal{W}_k)$ is the approximation in the ξ -th iteration and $p(\mathcal{W}, \mathbf{R})$ is the joint probability. $\mathbb{E}_{q^{(\xi)}(\mathcal{W}_{\setminus k})}$ means the expectation with respect the variational distributions excluding the variational distribution $q^{(\xi)}(\mathcal{W}_k)$. The approximated distribution $q(\mathcal{W}_k)$ in fact can be regarded as the approximation of the corresponding posterior distribution $p(\mathcal{W}_k | \mathbf{R})$. For example, $q(\mathbf{g})$ is the approximation to the posterior distribution $p(\mathbf{g} | \mathbf{R})$. Then the MAP estimation of each parameter \mathcal{W}_k can be achieved as

$$\mathcal{W}_k^{\text{MAP}} = \operatorname{argmax} q(\mathcal{W}_k). \quad (30)$$

To learn the tractable forms of variational distribution $q(\mathcal{W})$, we assume the prior distributions and the variational distribution follows the conjugate prior principles, which renders the variational distribution $q^{(\xi)}(\mathcal{W}_k)$ is identical to the prior distribution $p(\mathcal{W}_k)$ in form.

The proposed Bayesian framework can learn the true posterior distribution via the alternative optimization of the KL-divergence. Given the learning distribution, the channel parameters and localization can be done via posterior estimators. In the following subsections, the detailed variational distributions are derived and the user location is estimated iteratively via the estimation of other parameters.

C. Estimation of Channel Gains α_{au}

First, we consider the estimation problem of LOS channel gain α_{au} . According to (29), the ξ -th iteration variational distribution $q^{(\xi)}(\alpha_{au})$ can be given by

$$q^{(\xi)}(\alpha_{au}) \propto \exp \left\{ \mathbb{E}_{q^{(\xi)}(\mathcal{W}_{\setminus \alpha_{au}})} (\ln p(\mathbf{R}|\mathcal{W})) + \mathbb{E}_{q^{(\xi)}(\mathcal{W}_{\setminus \alpha_{au}})} (\ln p(\alpha_{au})) \right\}. \quad (31)$$

By plugging likelihood function in (19), the first variational expectation can be given by

$$\begin{aligned} & \mathbb{E}_{q^{(\xi)}(\mathcal{W}_{\setminus \alpha_{au}})} (\ln p(\mathbf{R}|\mathcal{W})) \\ &= \sum_{t=1}^T \mathbb{E}_{q^{(\xi)}(\mathcal{W}_{\setminus \alpha_{au}})} \text{tr} \left(-\frac{\Xi_{au}^H \Xi_{au} - 2(\mathbf{r}_t - \Xi_{ru}^t)^H \Xi_{au}}{2\delta} \right) \\ &+ \mathcal{C}, \end{aligned} \quad (32)$$

where \mathcal{C} are the terms that can be regarded as constant and

$$\mathbb{E}_{q^{(\xi)}(\mathcal{W}_{\setminus \alpha_{au}})} (\Xi_{au}^H \Xi_{au}) = \alpha_{au}^H \alpha_{au} P_w \mathcal{B}_{\zeta_{au}}^{(\xi)}, \quad (33)$$

where the scalar $\mathcal{B}_{\zeta_{au}}^{(\xi)} = \mathbb{E}_{q^{(\xi)}(\mathcal{W}_{\setminus \alpha_{au}})} (\varphi^H(\zeta_{au}) \varphi(\zeta_{au}))$ involves the expectation with respect to the nonlinear delay terms $\varphi(\zeta_{au})$ and the parameter $\mathcal{B}_{\zeta_{au}}^{(\xi)}$ can be given by

$$\begin{aligned} \mathcal{B}_{\zeta_{au}}^{(\xi)} &= \mathbb{E}_{q^{(\xi)}(\mathcal{W}_{\setminus \alpha_{au}})} (\varphi^H(\zeta_{au}) \varphi(\zeta_{au})) \\ &= \left(\boldsymbol{\mu}_{\varphi(\zeta_{au})}^{(\xi)} \right)^H \boldsymbol{\mu}_{\varphi(\zeta_{au})}^{(\xi)} + \text{tr} \left(\boldsymbol{\Sigma}_{\varphi(\zeta_{au})}^{(\xi)} \right), \end{aligned} \quad (34)$$

where $\boldsymbol{\mu}_{\varphi(\zeta_{au})}^{(\xi)}$ and $\boldsymbol{\Sigma}_{\varphi(\zeta_{au})}^{(\xi)}$ are the mean and variance of ξ -th distribution $q^{(\xi)}(\varphi(\zeta_{au}))$ and

$$q^{(\xi)}(\varphi(\zeta_{au})) = \mathcal{CN} \left(\varphi(\zeta_{au}) | \boldsymbol{\mu}_{\varphi(\zeta_{au})}^{(\xi)}, \boldsymbol{\Sigma}_{\varphi(\zeta_{au})}^{(\xi)} \right). \quad (35)$$

In (32), the expectation term $\mathbb{E}_{q^{(\xi)}(\mathcal{W}_{\setminus \alpha_{au}})} (\Xi_{au}^t)$ also involves the phase shift $\varphi(\zeta_{ru})$. Thus the expectation term $\mathbb{E}_{q^{(\xi)}(\mathcal{W}_{\setminus \alpha_{au}})} (\Xi_{au})$ is given by

$$\mathbb{E}_{q^{(\xi)}(\mathcal{W}_{\setminus \alpha_{au}})} (\Xi_{au}) = \alpha_{au} \sqrt{P_w} \boldsymbol{\mu}_{\varphi(\zeta_{au})}^{(\xi)}, \quad (36)$$

$$\mathbb{E}_{q^{(\xi)}(\mathcal{W}_{\setminus \alpha_{au}})} (\mathbf{r}_t - \Xi_{ru}^t) = \mathbf{r}_t - \underbrace{\sqrt{P_w} \boldsymbol{\mu}_{\varphi(\zeta_{ru})}^{(\xi)} \boldsymbol{\Upsilon}_t \mathbf{A} \boldsymbol{\mu}_{\Delta_{ru}}^{(\xi)}}_{\boldsymbol{\Theta}_{\alpha_{ru}}^{(t,\xi)}}, \quad (37)$$

where $\boldsymbol{\mu}_{\Delta_{ru}}^{(\xi)}$ is the mean of the variational distribution $q^{(\xi)}(\Delta_{ru})$ and is given by

$$\begin{aligned} q^{(\xi)}(\Delta_{ru}) &\propto \mathcal{CN} \left(\Delta_{ru} | \boldsymbol{\mu}_{\Delta_{ru}}^{(\xi)}, \boldsymbol{\Sigma}_{\Delta_{ru}}^{(\xi)} \right) \\ &= \prod_{i=1}^{\text{PQ}} \mathcal{CN} \left(\Delta_{ru}^i | \mu_{\Delta_{ru}^i}^{(\xi)}, \delta_{\Delta_{ru}^i}^{(\xi)} \right), \end{aligned} \quad (38)$$

$\boldsymbol{\mu}_{\varphi(\zeta_{ru})}^{(\xi)}$ is the mean vector of ξ -th distribution $q^{(\xi)}(\varphi(\zeta_{ru}))$ and

$$q^{(\xi)}(\varphi(\zeta_{ru})) = \mathcal{CN} \left(\varphi(\zeta_{ru}) | \boldsymbol{\mu}_{\varphi(\zeta_{ru})}^{(\xi)}, \boldsymbol{\Sigma}_{\varphi(\zeta_{ru})}^{(\xi)} \right). \quad (39)$$

Therefore, after simple manipulations, the expectation in (32) is given by

$$\begin{aligned} & \mathbb{E}_{q^{(\xi)}(\mathcal{W}_{\setminus \alpha_{au}})} (\ln p(\mathbf{R}|\mathcal{W})) \\ &= -\frac{1}{2} \alpha_{au}^H \Gamma_{\alpha_{au}}^{(\xi)} \alpha_{au} + \frac{1}{2} \left(\beta_{\alpha_{au}}^{(\xi)} \right)^H \alpha_{au} + \frac{1}{2} \alpha_{au}^H \beta_{\alpha_{au}}^{(\xi)} + \mathcal{C}, \end{aligned} \quad (40)$$

where $\beta_{\alpha_{au}}^{(\xi)} = \sum_{t=1}^T \frac{1}{\delta} \sqrt{P_w} \left(\boldsymbol{\mu}_{\varphi(\zeta_{au})}^{(\xi)} \right)^H \left(\mathbf{r}_t - \boldsymbol{\Theta}_{\alpha_{ru}}^{(t,\xi)} \right)$ and $\Gamma_{\alpha_{au}}^{(\xi)} = \frac{1}{\delta} T P_w \mathcal{B}_{\zeta_{au}}^{(\xi)}$.

By putting the prior distribution in (20), the another expectation term $\mathbb{E}_{q^{(\xi)}(\mathcal{W}_{\setminus \alpha_{au}})} (\ln p(\alpha_{au}))$ is given by

$$\begin{aligned} & \mathbb{E}_{q^{(\xi)}(\mathcal{W}_{\setminus \alpha_{au}})} (\ln p(\alpha_{au})) \\ &= -\frac{\alpha_{au}^H \alpha_{au}}{2\delta_{\alpha_{au}}} + \frac{\alpha_{au}^H \boldsymbol{\mu}_{\alpha_{au}}^H}{2\delta_{\alpha_{au}}} + \frac{\alpha_{au} \boldsymbol{\mu}_{\alpha_{au}}^H}{2\delta_{\alpha_{au}}} + \mathcal{C}. \end{aligned} \quad (41)$$

By inserting the equations (40) and (41) into (31), the ξ -th iteration variational distribution $q^{(\xi)}(\alpha_{au})$ in (31) can be given by

$$q^{(\xi)}(\alpha_{au}) \propto \mathcal{CN} \left(\alpha_{au} | \boldsymbol{\mu}_{\alpha_{au}}^{(\xi)}, \delta_{\alpha_{au}}^{(\xi)} \right), \quad (42)$$

where $\delta_{\alpha_{au}}^{(\xi)} = \left(\Gamma_{\varphi(\zeta_{au})}^{(\xi)} + \frac{1}{\delta_{\alpha_{au}}} \right)^{-1}$ and $\boldsymbol{\mu}_{\alpha_{au}}^{(\xi)} = \delta_{\alpha_{au}}^{(\xi)} \left(\frac{\boldsymbol{\mu}_{\alpha_{au}}}{\delta_{\alpha_{au}}} + \beta_{\alpha_{au}}^{(\xi)} \right)$.

D. Estimation of Phase shift $\varphi(\zeta_{au})$

The line-of-sight time delay ζ_{au} is nonlinear to the phase shift term $\varphi(\zeta_{au})$ and it is difficult to directly estimate the time delay ζ_{au} . Hence, we first estimate the nonlinear LOS phase shift $\varphi(\zeta_{au})$.

According to (29), the ξ -th iteration variational distribution $q^{(\xi)}(\varphi(\zeta_{au}))$ can be formulated

$$\begin{aligned} q^{(\xi)}(\varphi(\zeta_{au})) &\propto \exp \left\{ \mathbb{E}_{q^{(\xi)}(\mathcal{W}_{\setminus \varphi(\zeta_{au})})} (\ln p(\mathbf{R}|\mathcal{W})) \right. \\ &\left. + \mathbb{E}_{q^{(\xi)}(\mathcal{W}_{\setminus \varphi(\zeta_{au})})} (\ln p(\varphi(\zeta_{au}))) \right\}. \end{aligned} \quad (43)$$

Plugging the likelihood function (19) into the first expectation term $\mathbb{E}_{q^{(\xi)}(\mathcal{W}_{\setminus \varphi(\zeta_{au})})} (\ln p(\mathbf{R}|\mathcal{W}))$, it yields

$$\begin{aligned} & \mathbb{E}_{q^{(\xi)}(\mathcal{W}_{\setminus \varphi(\zeta_{au})})} (\ln p(\mathbf{R}|\mathcal{W})) \\ &= -\frac{1}{2\delta} \text{tr} \left(\varphi(\zeta_{au}) \varphi^H(\zeta_{au}) \boldsymbol{\Gamma}_{\varphi(\zeta_{au})}^{(\xi)} - 2 \left(\boldsymbol{\beta}_{\varphi(\zeta_{au})}^{(\xi)} \right)^H \varphi(\zeta_{au}) \right) \\ &+ \mathcal{C}, \end{aligned} \quad (44)$$

where \mathcal{C} is the terms irrelevant to the variable $\varphi(\zeta_{au})$ and can be regarded as constants. The other parameters are given by

$$\boldsymbol{\beta}_{\varphi(\zeta_{au})}^{(\xi)} = \sum_{t=1}^T \frac{1}{\delta} \left(\mathbf{r}_t - \boldsymbol{\Theta}_{\alpha_{ru}}^{(t,\xi)} \right)^H \alpha_{au}^{(\xi)} \sqrt{P_w}, \quad (45)$$

$$\boldsymbol{\Gamma}_{\varphi(\zeta_{au})}^{(\xi)} = T P_w \left(\left(\alpha_{au}^{(\xi)} \right)^H \alpha_{au}^{(\xi)} + \delta_{\alpha_{au}}^{(\xi)} \right), \quad (46)$$

and $\Theta_{\alpha_{ru}}^{(t,\xi)} = \sqrt{P_w} \boldsymbol{\mu}_{\varphi(\zeta_{ru})}^{(\xi)} \boldsymbol{\Upsilon}_t \mathcal{A} \boldsymbol{\mu}_{\Delta_{ru}}^{(\xi)} \cdot \boldsymbol{\mu}_{\Delta_{ru}}^{(\xi)}$ is the mean of the variational distribution $q^{(\xi)}(\Delta_{ru})$ and is given by

$$\begin{aligned} q^{(\xi)}(\Delta_{ru}) &\propto \mathcal{CN}\left(\Delta_{ru} | \boldsymbol{\mu}_{\Delta_{ru}}^{(\xi)}, \boldsymbol{\Sigma}_{\Delta_{ru}}^{(\xi)}\right) \\ &= \prod_{i=1}^{\text{PQ}} \mathcal{CN}\left(\Delta_{ru}^i | \mu_{\Delta_{ru}^i}^{(\xi)}, \delta_{\Delta_{ru}^i}^{(\xi)}\right), \end{aligned} \quad (47)$$

and $\boldsymbol{\mu}_{\varphi(\zeta_{ru})}^{(\xi)}$ is the mean vector of ξ -th distribution $q^{(\xi)}(\varphi(\zeta_{ru}))$ and

$$q^{(\xi)}(\varphi(\zeta_{ru})) = \mathcal{CN}\left(\varphi(\zeta_{ru}) | \boldsymbol{\mu}_{\varphi(\zeta_{ru})}^{(\xi)}, \boldsymbol{\Sigma}_{\varphi(\zeta_{ru})}^{(\xi)}\right), \quad (48)$$

will be given later.

Substituting (21) into the second expectation term $\mathbb{E}_{q^{(\xi)}(\varphi(\zeta_{au}))}(\ln p(\varphi(\zeta_{au})))$, it yields

$$\begin{aligned} &\mathbb{E}_{q^{(\xi)}(\varphi(\zeta_{au}))}(\ln p(\varphi(\zeta_{au}))) \\ &= -\frac{1}{2} \text{tr}\left(\boldsymbol{\varphi}^H(\zeta_{au}) \boldsymbol{\Sigma}_{\varphi(\zeta_{au})}^{-1} \boldsymbol{\varphi}(\zeta_{au})\right) \\ &\quad - 2\left(\boldsymbol{\mu}_{\varphi(\zeta_{au})}^{(\xi)}\right)^H \boldsymbol{\Sigma}_{\varphi(\zeta_{au})}^{-1} \boldsymbol{\varphi}(\zeta_{au}) + \mathcal{C}, \end{aligned} \quad (49)$$

By substituting (49) and (54) into (43), we can obtain

$$q^{(\xi)}(\varphi(\zeta_{au})) \propto \mathcal{CN}\left(\varphi(\zeta_{au}) | \boldsymbol{\mu}_{\varphi(\zeta_{au})}^{(\xi)}, \boldsymbol{\Sigma}_{\varphi(\zeta_{au})}^{(\xi)}\right), \quad (50)$$

where $\boldsymbol{\mu}_{\varphi(\zeta_{au})}^{(\xi)}$ and $\boldsymbol{\Sigma}_{\varphi(\zeta_{au})}^{(\xi)}$ are respectively given by

$$\boldsymbol{\mu}_{\varphi(\zeta_{au})}^{(\xi)} = \boldsymbol{\Sigma}_{\varphi(\zeta_{au})}^{(\xi)} \left(\boldsymbol{\mu}_{\varphi(\zeta_{au})}^H \boldsymbol{\Sigma}_{\varphi(\zeta_{au})}^{-1} + \boldsymbol{\beta}_{\varphi(\zeta_{au})}^{(\xi)} \right), \quad (51)$$

$$\boldsymbol{\Sigma}_{\varphi(\zeta_{au})}^{(\xi)} = \left(\boldsymbol{\Gamma}_{\varphi(\zeta_{au})}^{(\xi)} + \boldsymbol{\Sigma}_{\varphi(\zeta_{au})}^{-1} \right)^{-1}. \quad (52)$$

E. Estimation of Delay $\varphi(\zeta_{ru})$

The estimation of reflecting path time delay ζ_{ru} is similar to the estimation of $\varphi(\zeta_{ru})$ in subsection III-D. According to (29), the ξ -th iteration variational distribution $q^{(\xi)}(\varphi(\zeta_{ru}))$ is given by

$$\begin{aligned} q^{(\xi)}(\varphi(\zeta_{ru})) &\propto \exp\left\{ \mathbb{E}_{q^{(\xi)}(\boldsymbol{\mathcal{W}}_{\varphi(\zeta_{ru})})}(\ln p(\mathbf{R}|\boldsymbol{\mathcal{W}})) \right. \\ &\quad \left. + \mathbb{E}_{q^{(\xi)}(\boldsymbol{\mathcal{W}}_{\varphi(\zeta_{ru})})}(\ln p(\varphi(\zeta_{ru}))) \right\}. \end{aligned} \quad (53)$$

Substituting the likelihood function (19) into the first expectation term $\mathbb{E}_{q^{(\xi)}(\boldsymbol{\mathcal{W}}_{\varphi(\zeta_{ru})})}(\ln p(\mathbf{R}|\boldsymbol{\mathcal{W}}))$, it yields

$$\begin{aligned} &\mathbb{E}_{q^{(\xi)}(\boldsymbol{\mathcal{W}}_{\varphi(\zeta_{ru})})}(\ln p(\mathbf{R}|\boldsymbol{\mathcal{W}})) \\ &= -\frac{1}{2} \text{tr}\left(\boldsymbol{\varphi}(\zeta_{ru}) \boldsymbol{\varphi}^H(\zeta_{ru}) \boldsymbol{\Gamma}_{\varphi(\zeta_{ru})}^{(\xi)} - 2\left(\boldsymbol{\beta}_{\varphi(\zeta_{ru})}^{(\xi)}\right)^H \boldsymbol{\varphi}(\zeta_{ru})\right) \\ &\quad + \mathcal{C}, \end{aligned} \quad (54)$$

where with $\boldsymbol{\Gamma}_{\varphi(\zeta_{ru})}^{(\xi)}$ and $\boldsymbol{\beta}_{\varphi(\zeta_{ru})}^{(\xi)}$ are respectively given by

$$\begin{aligned} \boldsymbol{\Gamma}_{\varphi(\zeta_{ru})}^{(\xi)} &= \sum_{t=1}^T \mathbb{E}_{q^{(\xi)}(\boldsymbol{\mathcal{W}}_{\varphi(\zeta_{ru})})} \left(\frac{P_w}{\delta} \boldsymbol{\Upsilon}_t \mathcal{A} \Delta_{ru} \Delta_{ru}^H \boldsymbol{\Sigma}_{\Delta_{ru}}^{-1} \boldsymbol{\Upsilon}_t^H \right) \\ &= \sum_{t=1}^T \frac{P_w}{\delta} \boldsymbol{\Upsilon}_t \mathcal{A} \left(\boldsymbol{\mu}_{\Delta_{ru}}^{(\xi)} \left(\boldsymbol{\mu}_{\Delta_{ru}}^{(\xi)} \right)^H + \boldsymbol{\Sigma}_{\Delta_{ru}}^{(\xi)} \right) \boldsymbol{\Upsilon}_t^H, \end{aligned} \quad (55)$$

$$\boldsymbol{\beta}_{\varphi(\zeta_{ru})}^{(\xi)} = \sum_{t=1}^T \frac{1}{\delta} \left(\mathbf{r}_t - \Theta_{\alpha_{au}}^{(\xi)} \right) \sqrt{P_w} \left(\boldsymbol{\mu}_{\Delta_{ru}}^{(\xi)} \right)^H \boldsymbol{\Upsilon}_t^H. \quad (56)$$

where $\Theta_{\alpha_{au}}^{(\xi)} = \alpha_{au}^{(\xi)} \sqrt{P_w} \boldsymbol{\mu}_{\varphi(\zeta_{au})}^{(\xi)}$.

By putting the prior distribution (21) into the second expectation term, the second expectation term can be given by

$$\begin{aligned} &\mathbb{E}_{q^{(\xi)}(\varphi(\zeta_{ru}))}(\ln p(\varphi(\zeta_{ru}))) \\ &= -\frac{1}{2} \text{tr}\left(\boldsymbol{\varphi}^H(\zeta_{ru}) \boldsymbol{\Sigma}_{\varphi(\zeta_{ru})}^{-1} \boldsymbol{\varphi}(\zeta_{ru}) - 2\boldsymbol{\mu}_{\varphi(\zeta_{ru})}^H \boldsymbol{\Sigma}_{\varphi(\zeta_{ru})}^{-1} \boldsymbol{\varphi}(\zeta_{ru})\right) \\ &\quad + \mathcal{C}. \end{aligned} \quad (57)$$

Plugging (54) and (57) into (66) yields

$$q^{(\xi)}(\varphi(\zeta_{au})) \propto \mathcal{CN}\left(\varphi(\zeta_{au}) | \boldsymbol{\mu}_{\varphi(\zeta_{au})}^{(\xi)}, \boldsymbol{\Sigma}_{\varphi(\zeta_{au})}^{(\xi)}\right), \quad (58)$$

where

$$\boldsymbol{\mu}_{\varphi(\zeta_{ru})}^{(\xi)} = \boldsymbol{\Sigma}_{\varphi(\zeta_{ru})}^{(\xi)} \left(\boldsymbol{\mu}_{\varphi(\zeta_{ru})}^H \boldsymbol{\Sigma}_{\varphi(\zeta_{ru})}^{-1} + \boldsymbol{\beta}_{\varphi(\zeta_{ru})}^{(\xi)} \right), \quad (59)$$

$$\boldsymbol{\Sigma}_{\varphi(\zeta_{ru})}^{(\xi)} = \left(\boldsymbol{\Gamma}_{\varphi(\zeta_{ru})}^{(\xi)} + \boldsymbol{\Sigma}_{\varphi(\zeta_{ru})}^{-1} \right)^{-1}. \quad (60)$$

F. Estimation of Inverse Variance $w_{\Delta_{ru}^i}$

According to (29), the ξ -th iteration variational distribution $q^{(\xi)}(w_{\Delta_{ru}^i})$ is given by

$$\begin{aligned} q^{(\xi)}(w_{\Delta_{ru}^i}) &\propto \exp\left\{ \mathbb{E}_{q^{(\xi)}(\boldsymbol{\mathcal{W}}_{w_{\Delta_{ru}^i}})}(\ln p(\Delta_{ru}^i)) \right. \\ &\quad \left. + \mathbb{E}_{q^{(\xi)}(\boldsymbol{\mathcal{W}}_{w_{\Delta_{ru}^i}})}(\ln p(w_{\Delta_{ru}^i})) \right\}. \end{aligned} \quad (61)$$

Plugging (22) into the first expectation term in (61), it yields

$$\begin{aligned} &\mathbb{E}_{q^{(\xi)}(\boldsymbol{\mathcal{W}}_{w_{\Delta_{ru}^i}})}(\ln p(\Delta_{ru}^i)) \\ &= \mathbb{E}_{q^{(\xi)}(\boldsymbol{\mathcal{W}}_{w_{\Delta_{ru}^i}})} \left(\sum_{l=1}^2 g_{i,l} \ln \mathcal{CN}(\Delta_{ru}^i | \mu_{\Delta_{ru}^i}^l, w_{\Delta_{ru}^i}^{-1}) \right) \\ &= \frac{1}{2} \ln w_{\Delta_{ru}^i} - \varpi_i^{(\xi)} w_{\Delta_{ru}^i}, \end{aligned} \quad (62)$$

where $\varpi_i^{(\xi)} = \frac{1}{2} \sum_{l=1}^2 \tilde{h}_{i,l}^{(\xi)} \left(\left(\mu_{\Delta_{ru}^i}^{(\xi)} - \mu_{\Delta_{ru}^i}^l \right)^2 + \delta_{\Delta_{ru}^i}^{(\xi)} \right)$, and $\tilde{h}_{i,l}^{(\xi)}$ is the ξ -th estimated probability from the variational distribution $q^{(\xi)}(\mathbf{g})$.

The prior distribution is assumed to follow a Gamma distribution in (24) and the expectation term $\mathbb{E}_{q^{(\xi)}(\boldsymbol{\mathcal{W}}_{w_{\Delta_{ru}^i}})}(\ln p(w_{\Delta_{ru}^i}))$ is given by

$$\mathbb{E}_{q^{(\xi)}(\boldsymbol{\mathcal{W}}_{w_{\Delta_{ru}^i}})}(\ln p(w_{\Delta_{ru}^i})) = (a_i - 1) \ln w_{\Delta_{ru}^i} - \frac{1}{b_i} w_{\Delta_{ru}^i}. \quad (63)$$

With the results (62), (63), the variational distribution $q^{(\xi)}(w_{\Delta_{ru}^i})$ can be given by

$$q^{(\xi)}(w_{\Delta_{ru}^i}) \propto \Gamma\left(w_{\Delta_{ru}^i} | a_i^{(\xi)}, b_i^{(\xi)}\right), \quad (64)$$

where $a_i^{(\xi)} = a_i + \frac{1}{2}$ and $b_i^{(\xi)} = \left(\frac{1}{b_i} + \frac{\varpi_i^{(\xi)}}{2} \right)^{-1}$.

Hence, the ξ -th estimation of $w_{\Delta_{ru}^i}$ can be given by

$$w_{\Delta_{ru}^i}^{(\xi)} = a_i^{(\xi)} / b_i^{(\xi)}. \quad (65)$$

G. Estimation of Sparse Vector Δ_{ru}

The sparse vector Δ_{ru} is a one nonzero element vector and the nonzero element is the reflected path gain. Thus, the estimation of the sparse vector is equivalent to estimation of the reflected path gain α_{ru} . Meanwhile, the location of the nonzero element in the sparse vector Δ_{ru} determines the true steering vector in (16). Thus, the estimation of sparse vector Δ_{ru} has key impacts on the localization and channel estimation performance.

According to (29), the ξ -th iteration variational distribution $q^{(\xi)}(\Delta_{ru})$ is given by

$$q^{(\xi)}(\Delta_{ru}) \propto \exp \left\{ \mathbb{E}_{q^{(\xi)}(\mathcal{W}_{\setminus \Delta_{ru}})} (\ln p(\mathbf{R}|\mathcal{W})) + \mathbb{E}_{q^{(\xi)}(\mathcal{W}_{\setminus \Delta_{ru}})} (\ln p(\Delta_{ru})) \right\}. \quad (66)$$

Using similar steps, the first expectation term can be given by

$$\begin{aligned} & \mathbb{E}_{q^{(\xi)}(\mathcal{W}_{\setminus \Delta_{ru}})} (\ln p(\mathbf{R}|\mathcal{W})) \\ &= -\frac{1}{2} \left(\Delta_{ru}^H \mathcal{S}_{\Delta_{ru}}^{(\xi)} \Delta_{ru} - \left(\beta_{\Delta_{ru}}^{(\xi)} \right)^H \Delta_{ru} - \Delta_{ru}^H \beta_{\Delta_{ru}}^{(\xi)} \right) + \mathcal{C}, \end{aligned} \quad (67)$$

where $\mathcal{S}_{\Delta_{ru}}^{(\xi)}$ and $\beta_{\Delta_{ru}}^{(\xi)}$ are respectively given by

$$\begin{aligned} & \mathcal{S}_{\Delta_{ru}}^{(\xi)} \\ &= \sum_{t=1}^T \frac{1}{\delta} \mathbb{E}_{q^{(\xi)}(\mathcal{W}_{\setminus \Delta_{ru}})} \left(P_w \mathbf{A}^H \Upsilon_t^H \varphi^H(\zeta_{ru}) \varphi(\zeta_{ru}) \Upsilon_t \mathbf{A} \right), \\ &= \sum_{t=1}^T \frac{1}{\delta} \left(P_w \mathbf{A}^H \Upsilon_t^H \mathcal{B}_{\zeta_{ru}}^{(\xi)} \Upsilon_t \mathbf{A} \right) \end{aligned} \quad (68)$$

where the parameter $\beta_{\Delta_{ru}}^{(\xi)}$ is given by

$$\beta_{\Delta_{ru}}^{(\xi)} = \sum_{t=1}^T \frac{\sqrt{P_w}}{\delta} \mathbf{A}^H \Upsilon_t^H \left(\mu_{\varphi(\zeta_{ru})}^{(\xi)} \right)^H \left(\mathbf{r}_t - \Theta_{\alpha_{ru}}^{(\xi)} \right). \quad (69)$$

Substituting the prior distribution in (22) into the second expectation term, we can obtain

$$\begin{aligned} & \mathbb{E}_{q^{(\xi)}(\mathcal{W}_{\setminus \Delta_{ru}})} (\ln p(\Delta_{ru})) \\ &= \mathbb{E}_{q^{(\xi)}(\mathcal{W}_{\setminus \Delta_{ru}})} \left(\ln \left\{ \prod_{i=1}^{\text{PQ}} \prod_{l=1}^2 \mathcal{CN} \left(\Delta_{ru}^i | \mu_{\Delta}^l, w_{\Delta_{ru}^i}^{-1} \right)^{g_{i,l}} \right\} \right) \\ &= \\ & - \frac{1}{2} \sum_{i=1}^{\text{PQ}} \sum_{l=1}^2 \left(\Delta_{ru}^i - \mu_{\Delta}^l \right)^H \mathbb{E}_{q^{(\xi)}(\mathcal{W}_{\setminus \Delta_{ru}})} \left(g_{i,l} w_{\Delta_{ru}^i} \right) \left(\Delta_{ru} - \mu_{\Delta}^l \right) \\ & + \mathcal{C} \\ &= -\frac{1}{2} \sum_{l=1}^2 \left(\Delta_{ru} - \mu_{\Delta}^l \right)^H \mathbb{E}_{q^{(\xi)}(\mathcal{W}_{\setminus \Delta_{ru}})} \left(\Lambda_l \Sigma_{\Delta}^{-1} \right) \left(\Delta_{ru} - \mu_{\Delta}^l \right) \\ & + \mathcal{C} \end{aligned} \quad (70)$$

where $\Lambda_l = \text{diag} \{ g_{1,l}, \dots, g_{\text{PQ},l} \}$, $\Sigma_{\Delta} = \text{diag} \{ w_{\Delta_{ru}^1}^{-1}, \dots, w_{\Delta_{ru}^{\text{PQ}}}^{-1} \}$ and $\mathbf{g}_l = [g_{1,l}, \dots, g_{\text{PQ},l}]$ and

$$\begin{aligned} \mathcal{M}_l^{(\xi)} &= \mathbb{E}_{q^{(\xi)}(\mathcal{W}_{\setminus \Delta_{ru}})} \left(\Lambda_l \Sigma_{\Delta}^{-1} \right) \\ &= \text{diag} \left\{ \frac{a_1^{(\xi)}}{b_1^{(\xi)}} \tilde{h}_{1,l}^{(\xi)}, \dots, \frac{a_{\text{PQ}}^{(\xi)}}{b_{\text{PQ}}^{(\xi)}} \tilde{h}_{\text{PQ},l}^{(\xi)} \right\}. \end{aligned} \quad (71)$$

Substituting (71) into (70), the expectation term $\mathbb{E}_{q^{(\xi)}(\mathcal{W}_{\setminus \Delta_{ru}})} (\ln p(\Delta_{ru}))$ can be given by

$$\begin{aligned} & \mathbb{E}_{q^{(\xi)}(\mathcal{W}_{\setminus \Delta_{ru}})} (\ln p(\Delta_{ru})) \\ &= -\frac{1}{2} \left(\Delta_{ru}^H \Omega_{\Delta_{ru}}^{(\xi)} \Delta_{ru} - \Delta_{ru}^H \boldsymbol{\rho}_{\Delta_{ru}}^{(\xi)} - \left(\boldsymbol{\rho}_{\Delta_{ru}}^{(\xi)} \right)^H \Delta_{ru} \right) + \mathcal{C}, \end{aligned} \quad (72)$$

where $\Omega_{\Delta_{ru}}^{(\xi)} = \sum_{l=1}^2 \mathcal{M}_l^{(\xi)}$ and $\boldsymbol{\rho}_{\Delta_{ru}}^{(\xi)} = \sum_{l=1}^2 \mathcal{M}_l^{(\xi)} \boldsymbol{\mu}_{\Delta}^l$.

By plugging (67) and (72) in (66), the variational distribution $q^{(\xi)}(\Delta_{ru})$ is given by

$$q^{(\xi)}(\Delta_{ru}) \propto \mathcal{CN} \left(\Delta_{ru} | \boldsymbol{\mu}_{\Delta_{ru}}^{(\xi)}, \Sigma_{\Delta_{ru}}^{(\xi)} \right), \quad (73)$$

where $\boldsymbol{\mu}_{\Delta_{ru}}^{(\xi)}$ and $\Sigma_{\Delta_{ru}}^{(\xi)}$ are respectively given by

$$\boldsymbol{\mu}_{\Delta_{ru}}^{(\xi)} = \Sigma_{\Delta_{ru}}^{(\xi)} \left(\boldsymbol{\rho}_{\Delta_{ru}}^{(\xi)} + \boldsymbol{\beta}_{\Delta_{ru}}^{(\xi)} \right), \quad (74)$$

and

$$\Sigma_{\Delta_{ru}}^{(\xi)} = \left(\mathcal{S}_{\Delta_{ru}}^{(\xi)} + \Omega_{\Delta_{ru}}^{(\xi)} \right)^{-1}. \quad (75)$$

H. Estimation of Indicator \mathbf{g}

The indicator variable \mathbf{g} is directly involved with the sparse vector Δ_{ru} . The indicator variable indicates the location of the nonzero element in the sparse vector and the dependency is given in (23).

According to (29), the ξ -th iteration variational distribution $q^{(\xi)}(\mathbf{g})$ is given by

$$\begin{aligned} q^{(\xi)}(\mathbf{g}) &\propto \exp \left\{ \mathbb{E}_{q^{(\xi)}(\mathcal{W}_{\setminus \mathbf{g}})} (\ln p(\mathbf{g}|\mathcal{X})) \right. \\ & \left. + \mathbb{E}_{q^{(\xi)}(\mathcal{W}_{\setminus \mathbf{g}})} (\ln p(\Delta_{ru})) \right\}. \end{aligned} \quad (76)$$

Substituting (25) into the first expectation term into (76), we obtain the first expectation as

$$\mathbb{E}_{q^{(\xi)}(\mathcal{W}_{\setminus \mathbf{g}})} (\ln p(\mathbf{g}|\mathcal{X})) = \sum_{i=1}^{\text{PQ}} \sum_{l=1}^2 g_{i,l} \ln \chi_{i,l}. \quad (77)$$

Following the similar steps in (70), it yields

$$\begin{aligned} & \mathbb{E}_{q^{(\xi)}(\mathcal{W}_{\setminus \mathbf{g}})} (\ln p(\Delta_{ru})) \\ &= \sum_{i=1}^{\text{PQ}} \sum_{l=1}^2 g_{i,l} \ln \mathcal{CN} \left(\Delta_{ru}^i | \mu_{\Delta}^l, w_{\Delta_{ru}^i}^{-1} \right), \\ &= \sum_{i=1}^{\text{PQ}} \sum_{l=1}^2 g_{i,l} \mathcal{Q}_{i,l}^{(\xi)} \end{aligned} \quad (78)$$

where $\mu_{\Delta_{ru}^i}^{(\xi)}$ is the i -th element in $\boldsymbol{\mu}_{\Delta_{ru}}^{(\xi)}$. $\mathcal{Q}_{i,l}^{(\xi)} = \frac{1}{2} F \left(a_i^{(\xi)} \right) + \frac{1}{2} \ln \left(b_i^{(\xi)} \right) - \frac{1}{2} \left(\left(\mu_{\Delta_{ru}^i}^{(\xi)} - \mu_{\Delta}^l \right)^2 + \delta_{\Delta_{ru}^i}^{(\xi)} \right) a_i^{(\xi)} / b_i^{(\xi)}$ and $F(\cdot)$ is the digamma function.

Plugging (77) and (78) into (76) and considering the vector \mathbf{g} , it yields

$$q^{(\xi)}(\mathbf{g}) = \sum_{i=1}^{PQ} \sum_{l=1}^2 \left(\hat{h}_{i,l}^{(\xi)} \right)^{g_{i,l}}, \quad (79)$$

where $\hat{h}_{i,l}^{(\xi)} = \frac{\exp(\bar{Q}_{i,l}^{(\xi)})}{\sum_{l=1}^2 \exp(\bar{Q}_{i,l}^{(\xi)})}$ and $\bar{Q}_{i,l}^{(\xi)} = Q_{i,l}^{(\xi)} + \ln \chi_l$.

I. Estimation of UE Location

From the likelihood function in (12), it is computationally prohibitive to directly estimate the location of the user. Fortunately, the estimated location of the user can be given by $\mathbf{p}_u^{(\xi)} = \mathbf{p}_r + \rho \boldsymbol{\eta}^{(\xi)}$, where ρ is the distance between the UE and \mathbf{p}_r to be estimated. The vector $\boldsymbol{\eta}^{(\xi)} = -\frac{2\pi}{\lambda} [\sin \phi^{(\xi)} \cos \psi^{(\xi)}, \sin \phi^{(\xi)} \sin \psi^{(\xi)}, \cos \phi^{(\xi)}]^T$ is the waveform vector with the estimated azimuth and elevation angles. Moreover, the location follows the geometric constraints, which can be given by

$$\begin{aligned} (\zeta_{ru}^{(\xi)} - \zeta_{au}^{(\xi)}) c = & \underbrace{\left\| \rho \boldsymbol{\eta}^{(\xi)} \right\|_2}_{d_{ru}^{(\xi)}} + \underbrace{\left\| \mathbf{p}_a - \mathbf{p}_r \right\|_2}_{d_{ar}^{(\xi)}} - \\ & \underbrace{\left\| \mathbf{p}_a - \mathbf{p}_r - \rho \boldsymbol{\eta}^{(\xi)} \right\|_2}_{d_{au}^{(\xi)}}, \end{aligned} \quad (80)$$

where $\zeta_{ru}^{(\xi)}$ and $\zeta_{au}^{(\xi)}$ are the ξ -th estimation delays respectively. The delays ζ_{au} and ζ_{ru} can be estimated from $\boldsymbol{\mu}_{\varphi(\zeta_{au})}^{(\xi)}$ and $\boldsymbol{\mu}_{\varphi(\zeta_{ru})}^{(\xi)}$ respectively by following the results in [56]

$$\hat{\zeta}_{ru}^{(\xi)} = \arg \min_{\zeta_{ru}} \left\| \left(\boldsymbol{\mu}_{\varphi(\zeta_{ru})}^{(\xi)} \right)^H \boldsymbol{\mu}_{\varphi(\zeta_{ru})}^{(\xi)} \right\|_2, \quad (81)$$

and

$$\hat{\zeta}_{au}^{(\xi)} = \arg \min_{\zeta_{au}} \left\| \left(\boldsymbol{\mu}_{\varphi(\zeta_{au})}^{(\xi)} \right)^H \boldsymbol{\mu}_{\varphi(\zeta_{au})}^{(\xi)} \right\|_2. \quad (82)$$

Hence, the estimation of ρ can be obtained by minimizing

$$\rho^{(\xi)} = \arg \min_{\rho} \left\| \left(\zeta_{ru}^{(\xi)} - \zeta_{au}^{(\xi)} \right) c - d_{ru}^{(\xi)} - d_{ar}^{(\xi)} + d_{au}^{(\xi)} \right\|_2. \quad (83)$$

By taking derivative with respect to ρ and tedious manipulations, the solution $\rho^{(\xi)}$ is given by

$$\rho^{(\xi)} = \frac{\left(\left(\zeta_{ru}^{(\xi)} - \zeta_{au}^{(\xi)} \right) c - d_{ar}^{(\xi)} \right)^2 - \left(d_{ar}^{(\xi)} \right)^2}{2 \left(\left(\zeta_{ru}^{(\xi)} - \zeta_{au}^{(\xi)} \right) c - d_{ar}^{(\xi)} \right) \left\| \boldsymbol{\eta}^{(\xi)} \right\|^2 - 2 \left(\mathbf{p}_a - \mathbf{p}_r \right)^T \boldsymbol{\eta}^{(\xi)}} \quad (84)$$

Hence, the ξ -th estimation of the UE location is given by

$$\mathbf{p}_u^{(\xi)} = \mathbf{p}_r + \rho^{(\xi)} \boldsymbol{\eta}^{(\xi)}. \quad (85)$$

The user location and channel estimation involves various parameter estimation. For better and clearer presentation, we summarize the JCLE algorithm as **Algorithm I** and implementation interpretations are given by

- The time of flight (ToF) between the AP and RIS is hidden in the phase shift $\varphi(\zeta_{au})$. The ToF is estimated in subsections III-D;

- Similarly, the ToF between the RIS and the user is estimated in subsections III-E;
- The indicator \mathbf{g} is a key parameter that directly determines the angles of arrival and it is estimated in III-H;
- Given the estimated angles and ToFs, the user location can be determined in III-I.
- Nuisance parameters estimation are necessary to be included in the algorithm.

Our proposed algorithm is an iterative algorithm developed to approximate the true posterior distribution via mean-field factorization, KL divergence minimization, and alternating optimization. The convergence of the proposed variational Bayesian inference algorithm has been proven to converge [54, 55].

IV. DISCUSSIONS

In the paper, channel estimation and localization share commonalities in their reliance on received signal parameters and the utilization of signal processing techniques. Both processes involve extracting meaningful information from the transmitted signals to achieve their respective goals. For instance, the channel gains α_{au} and α_{ru} , delays ζ_{au} and ζ_{ru} , and angles ϕ and ψ are often used in both channel estimation and localization algorithms. However, they have distinct objectives: channel estimation focusing on characterizing the communication channel, and localization aiming to determine spatial locations. Their interdependence on shared signal characteristics highlights the synergy between these two vital components in wireless communication systems.

In **Algorithm I**, the complexity of the proposed algorithm mainly comes from the inversion in the covariance matrix when estimating of the sparse vector $\boldsymbol{\Delta}_{ru}$ in (75) in each iteration and other parameter estimation only involves scalars. The covariance matrix $\boldsymbol{\Sigma}_{\boldsymbol{\Delta}_{ru}}^{(\xi)}$ is with the dimension of $PQ \times PQ$ and the inversion will involve computational complexity of $\mathcal{O}\left((PQ)^3\right)$. First, the matrix $\mathbf{S}_{\boldsymbol{\Delta}_{ru}}^{(\xi)}$ can be reformulated as

$$\mathbf{S}_{\boldsymbol{\Delta}_{ru}}^{(\xi)} = \sum_{t=1}^T \frac{1}{\delta} \left(P_w \mathcal{A}^H \boldsymbol{\Upsilon}_t^H \mathcal{B}_{\zeta_{ru}}^{(\xi)} \boldsymbol{\Upsilon}_t \mathcal{A} \right) = \mathbf{F}^H \mathbf{F}, \quad (86)$$

with $\mathbf{F} = \sqrt{\frac{P_w \mathcal{B}_{\zeta_{ru}}^{(\xi)}}{\delta}} \boldsymbol{\Upsilon} \mathcal{A}$ and $\boldsymbol{\Upsilon} = [\boldsymbol{\Upsilon}_1, \boldsymbol{\Upsilon}_2, \dots, \boldsymbol{\Upsilon}_T]$.

Substituting (86) into (75) and utilizing the matrix inverse lemma, we can obtain

$$\begin{aligned} \boldsymbol{\Sigma}_{\boldsymbol{\Delta}_{ru}}^{(\xi)} &= \left(\mathbf{F}^H \mathbf{F} + \boldsymbol{\Omega}_{\boldsymbol{\Delta}_{ru}}^{(\xi)} \right)^{-1} \\ &= \left(\boldsymbol{\Omega}_{\boldsymbol{\Delta}_{ru}}^{(\xi)} \right)^{-1} \\ &\quad - \left(\boldsymbol{\Omega}_{\boldsymbol{\Delta}_{ru}}^{(\xi)} \right)^{-1} \mathbf{F}^H \left(\mathbf{I}^{-1} + \left(\boldsymbol{\Omega}_{\boldsymbol{\Delta}_{ru}}^{(\xi)} \right)^{-1} \right)^{-1} \mathbf{F} \left(\boldsymbol{\Omega}_{\boldsymbol{\Delta}_{ru}}^{(\xi)} \right)^{-1}, \end{aligned} \quad (87)$$

The computational complexity of estimating covariance matrix $\boldsymbol{\Sigma}_{\boldsymbol{\Delta}_{ru}}^{(\xi)}$ in (87) is reduced to $\mathcal{O}(TP^2Q^2)$. Hence, the total computational complexity of **Algorithm I** is proportional to $\mathcal{O}(TP^2Q^2)$. The complexity of the PSO algorithm is given by $\mathcal{O}(2LTS\eta)$, where S and η are the

particle number and the convergence iterations. The complexity of the ML algorithm mainly comes from the IFFT-based time delay estimation, which has the complexity of $\mathcal{O}(LT \log(LT) + MN \log(MN))$. Although the complexity of the proposed algorithm is possibly higher than that of the PSO and ML algorithms, our algorithm can achieve better localization performance, which will be demonstrated in the simulation section.

Algorithm 1 Variational Bayesian Inference-Based Localization and Channel Estimation Algorithm

- 1: Input the distributions $p(\alpha_{au})$, $p(\varphi(\zeta_{au}))$, $p(\varphi(\zeta_{ru}))$, $p(\Delta_{ru})$;
 - 2: Input the parameters δ , P_w , T , N , M , P , Q , \mathbf{p}_a , \mathbf{p}_u , \mathbf{p}_r and randomly generated ω , \mathcal{T} and collect measurements \mathbf{R} ;
 - 3: $\xi = 1$;
 - 4: **while** $|\text{KL}(q^{(\xi+1)}(\mathcal{W}) || p(\mathcal{W}|\mathbf{R})) - \text{KL}(q^{(\xi)}(\mathcal{W}) || p(\mathcal{W}|\mathbf{R}))| > \mathcal{T}$ **do** –
 - 5: Updating the mean $\mu_{\alpha_{au}}^{(\xi)}$ and variance $\delta_{\alpha_{au}}^{(\xi)}$ of $q^{(\xi)}(\alpha_{au})$ via (42) respectively;
 - 6: Updating the mean $\mu_{\varphi(\zeta_{au})}^{(\xi)}$ and variance $\Sigma_{\varphi(\zeta_{au})}^{(\xi)}$ of $q^{(\xi)}(\varphi(\zeta_{au}))$ via (51) and (52) respectively;
 - 7: Updating the mean $\mu_{\varphi(\zeta_{ru})}^{(\xi)}$ and variance $\Sigma_{\varphi(\zeta_{ru})}^{(\xi)}$ of $q^{(\xi)}(\varphi(\zeta_{ru}))$ via (59) and (60) respectively;
 - 8: Updating the mean $\mu_{\Delta_{ru}}^{(\xi)}$ and variance $\Sigma_{\Delta_{ru}}^{(\xi)}$ of $q^{(\xi)}(\Delta_{ru})$ via (74) and (75) respectively;
 - 9: Updating the parameters $\tilde{h}_{i,l}^{(\xi)}$ and $\tilde{Q}_{i,l}^{(\xi)}$ of $q^{(\xi)}(\mathbf{r})$ via (79) respectively;
 - 10: Updating the location $\mathbf{p}_u^{(\xi)}$ via (85);
 - 11: Output the ξ -th estimation of α_{au} , ζ_{au} , ζ_{ru} , Δ_{ru}^i , \mathbf{g}_i , χ and UE location \mathbf{p}_u via (51), (59), (74), $\chi_l^{(\xi)} = \frac{\lambda_l^{(\xi)}}{\sum_{i=1}^2 \lambda_i^{(\xi)}}$, (79), (85) respectively;
 - 12: $\xi = \xi + 1$;
 - 13: **end while**
-

V. SIMULATION RESULTS

A. Numerical Settings

In this section, we investigate the estimation performance of the proposed algorithm in different scenarios. Given the multiple channel parameters, the sparse vector Δ_{ru} estimation error and the angles estimation errors are presented to show the channel learning performance. We consider a 3D localization and channel estimation of a user with the aid of the RIS system. **The parameter settings are summarized as:**

TABLE I: **Parameter settings in simulation results**

Parameter	Value
\mathbf{p}_a	$[100, 100, 30]^T$
\mathbf{p}_r	$[10, 40, 10]^T$
M	20
N	20
P_w	1W
T	80
L	128
P	10
Q	10
δ	0.01

The distance between the RIS elements is half wavelength. The angle of arrivals ψ and ϕ range in $[-\frac{\pi}{2}, \frac{\pi}{2}]$. The prior parameters of unnormalized channel gain α_{au} is given by $\mu_{\alpha_{au}} = 0.2 + 0.2i$ and $\delta_{\alpha_{au}} = 0.01$. For the sparse vector Δ , the means are given by $\mu_{\Delta}^1 = 0$, $\mu_{\Delta}^2 = 0.5 + 0.5i$. $\mathbb{E}(w_{\Delta}^{-1}) = a_i b_i$, $a_i = 10^5$ and $b_i = 10^{-3}$. The initial positions of the user for all presented algorithms are both generated by adding Gaussian distributed bias $\mathcal{N}_p(\mathbf{0}, \tilde{\Sigma}_p)$ to the true position \mathbf{p}_r and $\tilde{\Sigma}_p = 25\mathbf{I}_3$. This prior information can be obtained via coarse estimation. The mentioned settings are unaltered and otherwise stated differently. For better clarification, the proposed algorithm is compared to the following algorithms:

- The quasi-Newton and maximum likelihood estimator were proposed for the localization problem in a RIS-aided localization system with the perfect channel information [38];
- A PSO algorithm was proposed to tackle the optimization problem for the RIS-aided localization in [36]. As a search algorithm, PSO can find the local optimum solutions of the proposed problem.
- Bayesian Cramer-Rao lower bound (BCRB): BCRB is adopted here as a benchmark for evaluating the performance of the proposed algorithm and the benchmark is derived using the Fisher information matrix. The original unknown parameter vector ϕ involves the other nuisance parameters and the Fisher information matrix is derived as [55, 57]

$$\begin{aligned}
 J(\mathcal{W}) &= \sum_{t=1}^T \mathbb{E}_{p(\mathbf{R}, \mathcal{W})} \left[\left(\frac{\partial \ln p(\mathbf{R}|\mathcal{W})}{\partial \mathcal{W}} \right)^H \frac{\partial \ln p(\mathbf{R}|\mathcal{W})}{\partial \mathcal{W}} \right] \\
 &+ \sum_{t=1}^T \mathbb{E}_{p(\mathbf{R}, \mathcal{W})} \left[\left(\frac{\partial \ln p(\mathcal{W})}{\partial \mathcal{W}} \right)^H \frac{\partial \ln p(\mathcal{W})}{\partial \mathcal{W}} \right], \\
 &\approx \frac{1}{\sigma} \sum_{t=1}^T \mathbb{E}_{p(\mathbf{R}, \mathcal{W})} \left[\Re \left(\frac{\partial \Xi_t^H}{\partial \mathcal{W}^H} \frac{\partial \Xi_t}{\partial \mathcal{W}} \right) \right]
 \end{aligned} \tag{88}$$

where $\Xi_t = \Xi_{au} + \Xi_{ru}^t$. The Fisher information matrix in (88) implies that the LOS and RIS signals both contribute to the estimation of channel gains and the angles. The prior distributions does not directly involve the UE position and can be ignored. For the localization error bound, we transform the unknown vector \mathcal{W} to an equivalent unknown variable vector $\kappa = [\mathbf{p}_u^T, \zeta_{ru}, \zeta_{au}, \psi, \phi]$ and the corresponding Fisher information matrix is given by

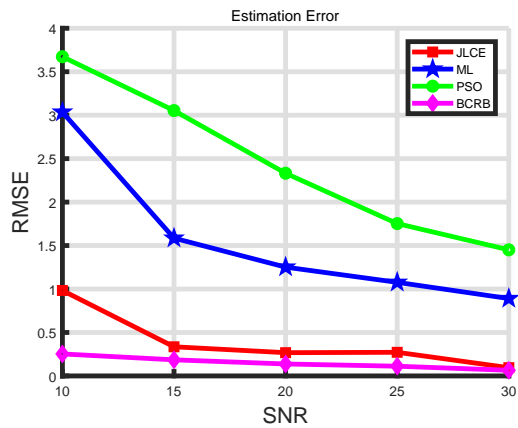


Fig. 2: Localization performances with OFDM subcarrier number $L = 128$ and snapshot $T = 80$ under different SNRs

[58]

$$J(\boldsymbol{\kappa}) = \mathcal{P}J(\mathcal{W})\mathcal{P}^T, \quad (89)$$

and \mathcal{P} is the transform matrix and given by $\mathcal{P} = \frac{\partial \mathcal{W}}{\partial \boldsymbol{\kappa}^T}$. Hence the equivalent Cramer-Rao lower bound of UE position is given by

$$\text{BCRB}_{\mathbf{p}_u} \geq \text{tr} \left([J^{-1}(\boldsymbol{\kappa})]_{1:3,1:3} \right). \quad (90)$$

where $[\bullet]_{1:3,1:3}$ is a block matrix composing of the first 3×3 elements in $J(\boldsymbol{\kappa})$. The detailed derivations of $J(\boldsymbol{\kappa})$ are given in Appendix A.

Using the results in (95), (97) and (98) in Appendix A, we can obtain

$$\text{BCRB}_{\mathbf{p}_u} \geq \sqrt{\text{tr} \left[\left(\mathbf{J}_{11} - \mathbf{J}_{12} \mathbf{J}_{22}^{-1} \mathbf{J}_{12}^T \right)^{-1} \right]}. \quad (91)$$

B. Far Field Scenarios

In this subsection, the numerical results of our algorithm in the far-field channel estimation and localization problem are investigated. The true user location is set to meet the constraint $\|\mathbf{p}_u - \mathbf{p}_r\|_2 = 20 > 100\lambda$ and λ is carrier wavelength.

In Fig.1, we first investigate the impact of signal-noise ratio (SNR) on the localization performance and estimation accuracy of the sparse vector $\boldsymbol{\Delta}_{ru}$. The PSO and ML algorithms both require the perfect knowledge of the reflected path channel gain α_{ru} and only the mean value of α_{ru} is available in this scenario. The particle number of the PSO algorithm is set to be 200. It is clear that the proposed algorithm JLCE can approach the BCRB with high SNR and the localization performance of the proposed algorithm JLCE outperforms the other algorithms. Because the proposed algorithm adopts the joint minimum mean square error (MMSE) estimation scheme and achieves accurate estimation of the sparse vector $\boldsymbol{\Delta}_{ru}$ and \mathbf{g} . Meanwhile, the estimation performance of the sparse vector $\boldsymbol{\Delta}_{ru}$ under different SNRs is also investigated in Fig.2. The proposed algorithm can achieve stable convergence at a rapid rate (less than 5 iterations). The results in Fig.2 and Fig.3 both intuitively show that the localization and estimation performances will increase with the higher SNR and the proposed algorithm can achieve better performances.

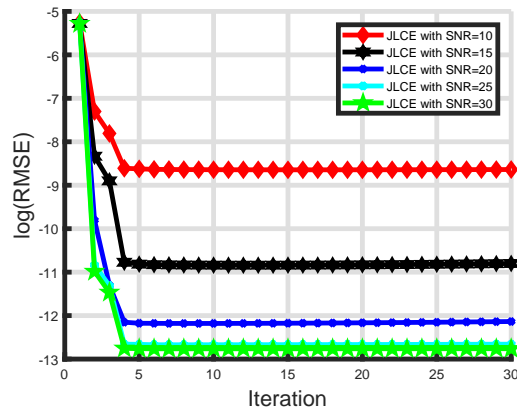


Fig. 3: Sparse channel vector $\boldsymbol{\Delta}_{ru}$ estimation results with $L = 128$ and snapshot $T = 80$ under different SNRs

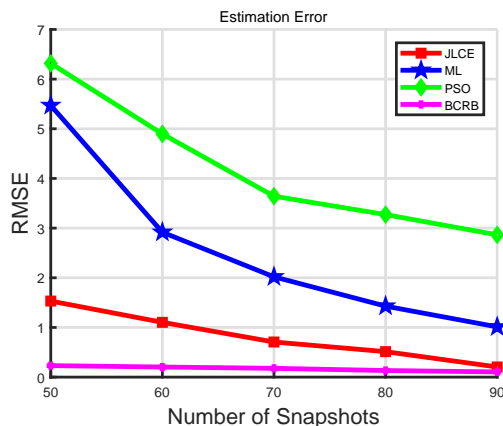


Fig. 4: Localization performances with SNR = 15 dB and $L = 128$ under different snapshots

In Fig.4 and Fig.5, the joint localization and channel estimation problem with different snapshot numbers is investigated. The results in Fig.4 and Fig.5 also support similar conclusions that demonstrate the superiority of the proposed algorithm in localization accuracy, estimation performance as well as convergence rate. Besides, the augmentation of the snapshot number with fixed PQ means the ratio T/PQ changes. The ratio approaching 1 means the matrix $\Upsilon \mathbf{A}$ is becoming a full sampling matrix.

For the channel parameter estimation performances, the estimation errors can be reduced by increasing the snapshot T or SNR in Fig.3 and Fig.5. The vector $\boldsymbol{\Delta}_{ru}$ is the sparse representation of the reflected path gain α_{ru} . The simulation results indicated that the proposed algorithm can precisely estimate the channel parameters simultaneously. Furthermore, we also investigated the azimuth and elevation angle estimation performances in Fig.6. The simulation results showed the proposed algorithm can accurately estimate the angles in a few iterations. Meanwhile, the off-grid errors were ignored given enough PQ and it leads to zero estimation errors in Fig.6. Given the intuitive analysis and simulation results, the robustness and validity of the proposed algorithm in estimating the channel state information was verified.

In Fig.7, the localization performance is investigated under different numbers of RIS elements and other parameters

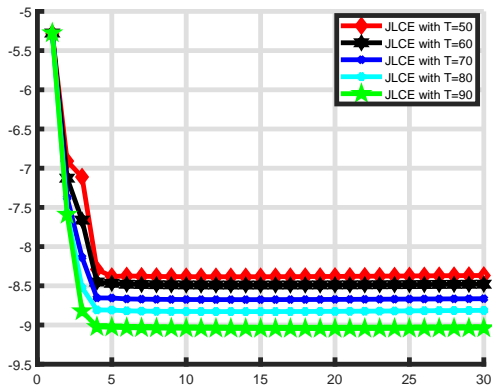


Fig. 5: Sparse channel vector $\Delta_{r,u}$ estimation results with SNR = 15 dB and $L = 128$ under different snapshots

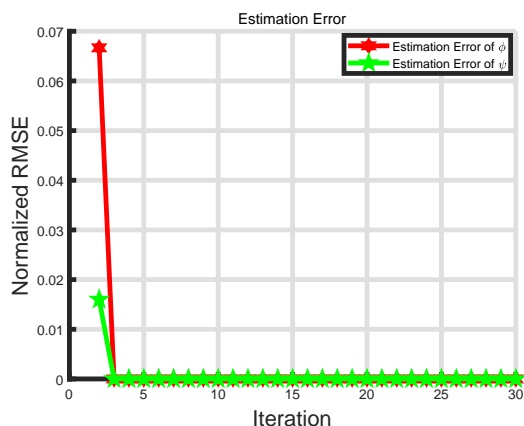


Fig. 6: Azimuth and elevation angles estimation errors with SNR = 15 dB, $L = 128$ and $T = 70$

remain unaltered. The number of RIS elements is set to be $M \times N$ with $M = N$. With the augmentation of the RIS element number, the localization accuracy of the JCLE algorithm and the BCRB both decrease and achieve better performance, which demonstrates that the RIS can benefit the localization systems. Moreover, the BCRB and localization error both indicated that there existed a tradeoff between the number of RIS elements and the computational complexity.

C. Near Field Scenarios

The numerical results of our algorithm in the near-field channel estimation and localization problem are also investigated. The true user location is set to meet the constraint $\|\mathbf{p}_u - \mathbf{p}_r\|_2 \leq 100\lambda$ and λ is carrier wavelength by following the near-filed settings in [43].

The simulation results in Fig.8 and Fig.10 present the localization performances of the proposed algorithm and other algorithms in the near-filed scenarios. The proposed algorithm can also approach the localization accuracy benchmark BCRB and outperform other compared algorithms. The numerical results in Fig.9 show the estimation error of the sparse vector in the near-field scenario, which also shows that the

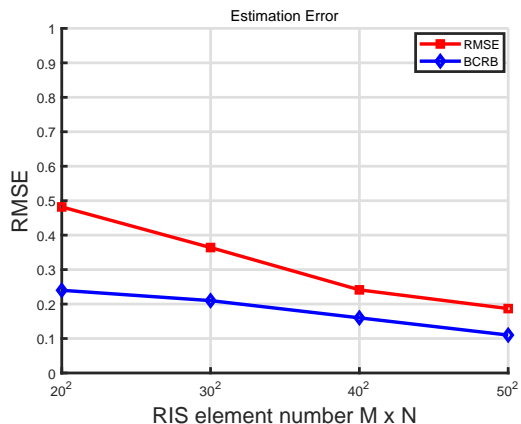


Fig. 7: Localization performance with SNR = 15dB, $T = 80$ and $L = 128$ with different number of RIS elements $M \times N$

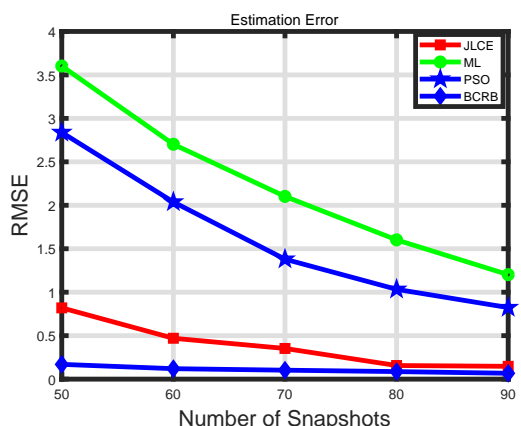


Fig. 8: Localization performance with SNR = 15dB and $L = 128$ under different number of snapshots

proposed algorithm can achieve accurate estimation of channel parameters. The results in near-filed and far-filed scenarios both demonstrate the superiority of the proposed algorithm in localization and validity in channel semation.

VI. CONCLUSION

In the paper, we considered a joint localization and channel estimation problem in the RIS-aided system and we proposed a JLCE algorithm to study the complicated estimation problem. Due to the intractable direct maximization of the objective function, the true posterior distribution is approximated by a joint variational distribution iteratively. In the proposed iterative algorithm, we also investigated the algorithm complexity and convergence. Simulation results have shown the superiority of the proposed algorithm in channel estimation and localization accuracy through various simulation examples.

APPENDIX A

The transformation matrix $\mathcal{P} = \frac{\partial \mathcal{Y}}{\partial \kappa^T}$ can be calculated as

$$\mathcal{P} = \begin{bmatrix} \mathcal{P}_{11} & \mathbf{0} \\ \mathbf{0} & \mathcal{P}_{22} \end{bmatrix} \in \mathbb{C}^{7 \times (2L+2PQ+2)}, \quad (92)$$

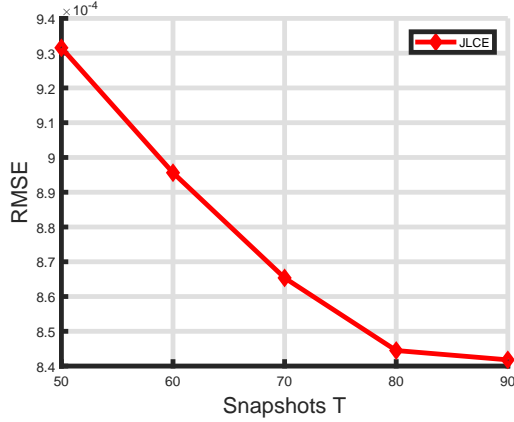


Fig. 9: Sparse channel vector Δ_{ru} estimation results with SNR = 15 dB and $L = 128$ under different number of snapshots

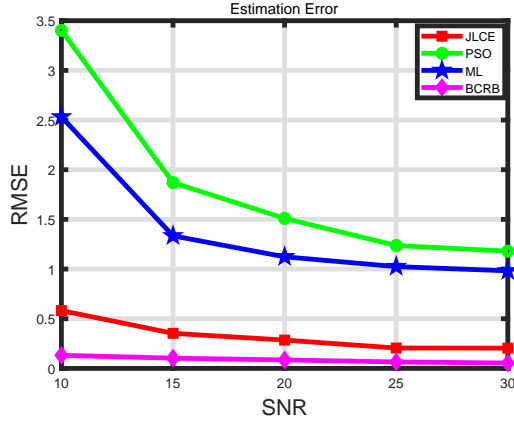


Fig. 10: Localization performance with snapshot $T = 70$ and $L = 128$ with different SNRs

where $\mathcal{P}_{11} = \begin{bmatrix} \frac{\partial \varphi^H(\zeta_{au})}{\partial \mathbf{p}_u} & \frac{\partial \varphi^T(\zeta_{au})}{\partial \zeta_{au}} & \mathbf{0}_{1 \times L} \\ \frac{\partial \varphi^H(\zeta_{ru})}{\partial \mathbf{p}_u} & \mathbf{0}_{1 \times L} & \frac{\partial \varphi^H(\zeta_{ru})}{\partial \zeta_{ru}} \end{bmatrix}^T$ and

$$\mathcal{P}_{22} = \begin{bmatrix} 0 & 1 & \mathbf{0}_{1 \times PQ} & \mathbf{0}_{1 \times PQ} \\ 1 & 0 & \mathbf{0}_{1 \times PQ} & \mathbf{0}_{1 \times PQ} \end{bmatrix}^T.$$

The term $\frac{\partial \Xi_t}{\partial \mathcal{W}}$ requires the derivative of $\frac{\partial \Xi_{au}}{\partial \mathcal{W}}$ and $\frac{\partial \Xi_{ru}^t}{\partial \mathcal{W}}$. $\frac{\partial \Xi_{au}}{\partial \mathcal{W}} = [\alpha_{au} \sqrt{P_w} \mathbf{I}_L, \mathbf{0}] \in \mathbb{C}^{L \times (2L+2PQ+2)}$. Similarly $\frac{\partial \Xi_{ru}^t}{\partial \mathcal{W}} = [\mathbf{0}, \mathcal{M}^t, \frac{\partial \Xi_{ru}^t}{\partial \psi}, \frac{\partial \Xi_{ru}^t}{\partial \phi}, \mathbf{0}, \mathbf{0}] \in \mathbb{C}^{L \times (2L+2+2PQ)}$ with

$$\mathcal{M}^t = \alpha_{ru} \sqrt{P_w} \mathbf{a}^T(\theta, \vartheta) \text{diag}(\Omega_t) \mathbf{a}(\psi, \phi) \mathbf{I}_L. \quad (93)$$

Expanding the product term $\frac{\partial \Xi_t^H}{\partial \mathcal{W}^H} \frac{\partial \Xi_t}{\partial \mathcal{W}}$ and substituting $\frac{\partial \Xi_{au}}{\partial \mathcal{W}}$ and $\frac{\partial \Xi_{ru}^t}{\partial \mathcal{W}}$ into (88), we obtain

$$\mathbf{J}(\mathcal{W}) = \mathbb{E}_{p(\mathbf{R}, \mathcal{W})} \begin{bmatrix} \alpha_{au}^2 P_w \mathbf{I}_L & \mathbf{J}_{ar} & \mathbf{0} \\ \mathbf{J}_{ar}^H & \mathcal{R} & \mathbf{0} \\ \mathbf{0} & \mathbf{0} & \mathbf{0} \end{bmatrix}, \quad (94)$$

where $\mathbf{J}_{ar} = \mathbb{E}_{p(\mathbf{R}, \mathcal{W})} (\alpha_{au} \sqrt{P_w} \mathbf{I}_L \mathbf{Q}^t) = \mathcal{G} \mathbf{Q}^t$, $\mathbf{Q}^t = \begin{bmatrix} \Re(\mathcal{M}^t) & \Re(\frac{\partial \Xi_{ru}^t}{\partial \psi}) & \Re(\frac{\partial \Xi_{ru}^t}{\partial \phi}) \end{bmatrix}$ and $\mathcal{R} = \mathbb{E}_{p(\mathbf{R}, \mathcal{W})} ((\mathbf{Q}^t)^H \mathbf{Q}^t)$.

Substituting (92) and (94) into (89), it yields

$$\mathbf{J}(\boldsymbol{\kappa}) = \begin{bmatrix} \mathbf{J}_{11} & \mathbf{J}_{12} \\ \mathbf{J}_{12}^T & \mathbf{J}_{22} \end{bmatrix}, \quad (95)$$

where the submatrices are given by $\mathbf{J}_{11} = \mathbf{U}^H \mathbf{U} + \delta_{\alpha_{au}} \frac{\partial \varphi(\zeta_{ru})}{\partial \mathbf{p}_u} \frac{\partial \varphi^H(\zeta_{ru})}{\partial \mathbf{p}_u}$ with $\mathbf{U} = (\mathcal{G} + \mathcal{M}^t)^H \frac{\partial \varphi^H(\zeta_{ru})}{\partial \mathbf{p}_u}$.

$$\mathbf{J}_{12} = \begin{bmatrix} \frac{\partial \varphi^H(\zeta_{au})}{\partial \mathbf{p}_u} (\tilde{\mathcal{G}} + \mathcal{G}(\mathcal{M}^t)^H) \frac{\partial \varphi(\zeta_{au})}{\partial \zeta_{au}} \\ \frac{\partial \varphi^H(\zeta_{au})}{\partial \mathbf{p}_u} (\tilde{\mathcal{G}}(\mathcal{M}^t)^H + (\mathcal{M}^t)^H \mathcal{M}^t) \frac{\partial \varphi(\zeta_{ru})}{\partial \zeta_{ru}} \\ \frac{\partial \varphi^H(\zeta_{au})}{\partial \mathbf{p}_u} (\mathcal{G}(\mathcal{M}^t)^H + \mathcal{M}^t) \left(\frac{\partial \Xi_{ru}^t}{\partial \psi} \right)^H \\ \frac{\partial \varphi^H(\zeta_{au})}{\partial \mathbf{p}_u} (\mathcal{G}(\mathcal{M}^t)^H + \mathcal{M}^t) \left(\frac{\partial \Xi_{ru}^t}{\partial \phi} \right)^H \end{bmatrix}, \quad (96)$$

with $\tilde{\mathcal{G}} = \mathcal{G} \mathcal{G}^H + \delta_{\alpha_{au}} \mathbf{I}_L$ and $\mathbf{J}_{22} = \mathcal{F} \mathcal{D} \mathcal{F}^H$, where

$$\mathcal{F} = \begin{bmatrix} \frac{\partial \varphi^H(\zeta_{au})}{\partial \zeta_{au}} & \frac{\partial \varphi^H(\zeta_{ru})}{\partial \zeta_{ru}} & \frac{\partial \Xi_{ru}^t}{\partial \psi} & \frac{\partial \Xi_{ru}^t}{\partial \phi} \\ \mathbf{0} & \mathbf{0} & \mathbf{0} & \mathbf{0} \end{bmatrix}^H, \quad (97)$$

and

$$\mathcal{D} = \begin{bmatrix} \tilde{\mathcal{G}} & \mathcal{G} \mathcal{M}^t & \mathcal{G} & (\mathcal{G}^t)^H \\ (\mathcal{M}^t)^H \mathcal{G} & (\mathcal{M}^t)^H \mathcal{M}^t & (\mathcal{M}^t)^H & (\mathcal{M}^t)^H \\ \mathcal{G} & \mathcal{M}^t & \mathbf{1} & (\mathcal{M}^t)^H \\ \mathcal{G}^t & \mathcal{M}^t & (\mathcal{M}^t)^H & \mathbf{1} \end{bmatrix}. \quad (98)$$

REFERENCES

- [1] Y. Zhu, H. Guo, and V. K. N. Lau, "Bayesian channel estimation in multi-user massive MIMO with extremely large antenna array," *IEEE Transactions on Signal Processing*, vol. 69, pp. 5463–5478, 2021.
- [2] R. Zhang, B. Shim, and W. Wu, "Direction-of-arrival estimation for large antenna arrays with hybrid analog and digital architectures," *IEEE Transactions on Signal Processing*, vol. 70, pp. 72–88, 2022.
- [3] J. Yang, Y. Zeng, S. Jin, C.-K. Wen, and P. Xu, "Communication and localization with extremely large lens antenna array," *IEEE Transactions on Wireless Communications*, vol. 20, no. 5, pp. 3031–3048, 2021.
- [4] M. A. ElMossallamy, H. Zhang, L. Song, K. G. Seddik, Z. Han, and G. Y. Li, "Reconfigurable intelligent surfaces for wireless communications: Principles, challenges, and opportunities," *IEEE Transactions on Cognitive Communications and Networking*, vol. 6, no. 3, pp. 990–1002, 2020.
- [5] H. Guo, Y.-C. Liang, J. Chen, and E. G. Larsson, "Weighted sum-rate maximization for reconfigurable intelligent surface aided wireless networks," *IEEE Transactions on Wireless Communications*, vol. 19, no. 5, pp. 3064–3076, 2020.
- [6] G. Zhou, C. Pan, H. Ren, K. Wang, and Z. Peng, "Secure wireless communication in RIS-aided MISO system with hardware impairments," *IEEE Wireless Communications Letters*, vol. 10, no. 6, pp. 1309–1313, 2021.
- [7] Y. Li, S. Ma, G. Yang, and K.-K. Wong, "Secure localization and velocity estimation in mobile iot networks

- with malicious attacks,” *IEEE Internet of Things Journal*, vol. 8, no. 8, pp. 6878–6892, 2021.
- [8] H. Zhang, S. Ma, Z. Shi, X. Zhao, and G. Yang, “Sum-rate maximization of RIS-aided multi-user MIMO systems with statistical CSI,” *IEEE Transactions on Wireless Communications*, pp. 1–1, 2022.
- [9] A. Bhowal and S. Aïssa, “RIS-aided communications in indoor and outdoor environments: Performance analysis with a realistic channel model,” *IEEE Transactions on Vehicular Technology*, vol. 71, no. 12, pp. 13 356–13 360, 2022.
- [10] Z. Chen, G. Chen, J. Tang, S. Zhang, D. K. So, O. A. Dobre, K.-K. Wong, and J. Chambers, “Reconfigurable-intelligent-surface-assisted B5G/6G wireless communications: Challenges, solution, and future opportunities,” *IEEE Communications Magazine*, vol. 61, no. 1, pp. 16–22, 2023.
- [11] M. Di Renzo, A. Zappone, M. Debbah, M.-S. Alouini, C. Yuen, J. de Rosny, and S. Tretyakov, “Smart radio environments empowered by reconfigurable intelligent surfaces: How it works, state of research, and the road ahead,” *IEEE Journal on Selected Areas in Communications*, vol. 38, no. 11, pp. 2450–2525, 2020.
- [12] H. Gacanin and M. Di Renzo, “Wireless 2.0: Toward an intelligent radio environment empowered by reconfigurable meta-surfaces and artificial intelligence,” *IEEE Vehicular Technology Magazine*, vol. 15, no. 4, pp. 74–82, 2020.
- [13] B. Teng, X. Yuan, R. Wang, and S. Jin, “Bayesian user localization and tracking for reconfigurable intelligent surface aided MIMO systems,” *IEEE Journal of Selected Topics in Signal Processing*, vol. 16, no. 5, pp. 1040–1054, 2022.
- [14] X. Gan, C. Zhong, C. Huang, and Z. Zhang, “RIS-assisted multi-user MISO communications exploiting statistical CSI,” *IEEE Transactions on Communications*, vol. 69, no. 10, pp. 6781–6792, 2021.
- [15] C. Huang, Z. Yang, G. C. Alexandropoulos, K. Xiong, L. Wei, C. Yuen, Z. Zhang, and M. Debbah, “Multi-hop RIS-empowered Terahertz communications: A drl-based hybrid beamforming design,” *IEEE Journal on Selected Areas in Communications*, vol. 39, no. 6, pp. 1663–1677, 2021.
- [16] A. L. Swindlehurst, G. Zhou, R. Liu, C. Pan, and M. Li, “Channel estimation with reconfigurable intelligent surfaces—a general framework,” *Proceedings of the IEEE*, vol. 110, no. 9, pp. 1312–1338, 2022.
- [17] S. Ma, W. Shen, X. Gao, and J. An, “Robust channel estimation for RIS-aided millimeter-wave system with RIS blockage,” *IEEE Transactions on Vehicular Technology*, vol. 71, no. 5, pp. 5621–5626, 2022.
- [18] X. Pei, H. Yin, L. Tan, L. Cao, Z. Li, K. Wang, K. Zhang, and E. Björnson, “RIS-aided wireless communications: Prototyping, adaptive beamforming, and indoor/outdoor field trials,” *IEEE Transactions on Communications*, vol. 69, no. 12, pp. 8627–8640, 2021.
- [19] H. Jiang, B. Xiong, H. Zhang, and E. Basar, “Hybrid far- and near-field modeling for reconfigurable intelligent surface assisted V2V channels: A sub-array partition based approach,” *IEEE Transactions on Wireless Communications*, vol. 22, no. 11, pp. 8290–8303, 2023.
- [20] M. Cui, Z. Wu, Y. Lu, X. Wei, and L. Dai, “Near-field MIMO communications for 6G: Fundamentals, challenges, potentials, and future directions,” *IEEE Communications Magazine*, vol. 61, no. 1, pp. 40–46, 2023.
- [21] Y. Pan, C. Pan, S. Jin, and J. Wang, “RIS-aided near-field localization and channel estimation for the Terahertz system,” *IEEE Journal of Selected Topics in Signal Processing*, vol. 17, no. 4, pp. 878–892, 2023.
- [22] A. Guerra, F. Guidi, D. Dardari, and P. M. Djurić, “Near-field tracking with large antenna arrays: Fundamental limits and practical algorithms,” *IEEE Transactions on Signal Processing*, vol. 69, pp. 5723–5738, 2021.
- [23] J. He, H. Wymeersch, and M. Juntti, “Channel estimation for RIS-aided mmwave MIMO systems via atomic norm minimization,” *IEEE Transactions on Wireless Communications*, vol. 20, no. 9, pp. 5786–5797, 2021.
- [24] X. Wei, D. Shen, and L. Dai, “Channel estimation for RIS assisted wireless communications —part II: An improved solution based on double-structured sparsity,” *IEEE Communications Letters*, vol. 25, no. 5, pp. 1403–1407, 2021.
- [25] K. Ardah, S. Gherekhloo, A. L. F. de Almeida, and M. Haardt, “TRICE: A channel estimation framework for RIS-aided Millimeter-Wave MIMO systems,” *IEEE Signal Processing Letters*, vol. 28, pp. 513–517, 2021.
- [26] H. Liu, X. Yuan, and Y.-J. A. Zhang, “Matrix-calibration-based cascaded channel estimation for reconfigurable intelligent surface assisted multiuser MIMO,” *IEEE Journal on Selected Areas in Communications*, vol. 38, no. 11, pp. 2621–2636, 2020.
- [27] Y. Liu, S. Zhang, F. Gao, J. Tang, and O. A. Dobre, “Cascaded channel estimation for RIS assisted mmWave MIMO transmissions,” *IEEE Wireless Communications Letters*, pp. 1–1, 2021.
- [28] L. Wei, C. Huang, G. C. Alexandropoulos, C. Yuen, Z. Zhang, and M. Debbah, “Channel estimation for RIS-empowered multi-user MISO wireless communications,” *IEEE Transactions on Communications*, vol. 69, no. 6, pp. 4144–4157, 2021.
- [29] Z. Zhou, N. Ge, Z. Wang, and L. Hanzo, “Joint transmit precoding and reconfigurable intelligent surface phase adjustment: A decomposition-aided channel estimation approach,” *IEEE Transactions on Communications*, vol. 69, no. 2, pp. 1228–1243, 2021.
- [30] C. You, B. Zheng, and R. Zhang, “Channel estimation and passive beamforming for intelligent reflecting surface: Discrete phase shift and progressive refinement,” *IEEE Journal on Selected Areas in Communications*, vol. 38, no. 11, pp. 2604–2620, 2020.
- [31] M. Li, S. Zhang, Y. Ge, F. Gao, and P. Fan, “Joint channel estimation and data detection for hybrid RIS aided millimeter wave OTFS systems,” *IEEE Transactions on Communications*, vol. 70, no. 10, pp. 6832–6848, 2022.
- [32] A. Papazafeiropoulos, C. Pan, P. Kourtessis, S. Chatzinothas, and J. M. Senior, “Intelligent reflecting surface-

- assisted MU-MISO systems with imperfect hardware: Channel estimation and beamforming design,” *IEEE Transactions on Wireless Communications*, vol. 21, no. 3, pp. 2077–2092, 2022.
- [33] H. Wymeersch, J. He, B. Denis, A. Clemente, and M. Juntti, “Radio localization and mapping with reconfigurable intelligent surfaces: Challenges, opportunities, and research directions,” *IEEE Vehicular Technology Magazine*, vol. 15, no. 4, pp. 52–61, 2020.
- [34] T. Ma, Y. Xiao, X. Lei, W. Xiong, and Y. Ding, “Indoor localization with reconfigurable intelligent surface,” *IEEE Communications Letters*, vol. 25, no. 1, pp. 161–165, 2021.
- [35] G. Ghatak, “On the placement of intelligent surfaces for RSSI-based ranging in Mm-wave networks,” *IEEE Communications Letters*, vol. 25, no. 6, pp. 2043–2047, 2021.
- [36] H. Zhang, H. Zhang, B. Di, K. Bian, Z. Han, and L. Song, “Metalocalization: Reconfigurable intelligent surface aided multi-user wireless indoor localization,” *IEEE Transactions on Wireless Communications*, pp. 1–1, 2021.
- [37] —, “Towards ubiquitous positioning by leveraging reconfigurable intelligent surface,” *IEEE Communications Letters*, vol. 25, no. 1, pp. 284–288, 2021.
- [38] K. Keykhosravi, M. F. Keskin, G. Seco-Granados, and H. Wymeersch, “SISO RIS-enabled joint 3D downlink localization and synchronization,” in *ICC 2021 - IEEE International Conference on Communications*, 2021, pp. 1–6.
- [39] A. Elzanaty, A. Guerra, F. Guidi, and M. Alouini, “Reconfigurable intelligent surfaces for localization: Position and orientation error bounds,” *IEEE Transactions on Signal Processing*, pp. 1–1, 2021.
- [40] H. Wymeersch and B. Denis, “Beyond 5G wireless localization with reconfigurable intelligent surfaces,” in *ICC 2020 - 2020 IEEE International Conference on Communications (ICC)*, 2020, pp. 1–6.
- [41] J. Zhang, Z. Zheng, Z. Fei, and X. Bao, “Positioning with dual reconfigurable intelligent surfaces in millimeter-wave MIMO systems,” in *2020 IEEE/CIC International Conference on Communications in China (ICCC)*, 2020, pp. 800–805.
- [42] Y. Lin, S. Jin, M. Matthaiou, and X. You, “Channel estimation and user localization for IRS-assisted MIMO-OFDM systems,” *IEEE Transactions on Wireless Communications*, vol. 21, no. 4, pp. 2320–2335, 2022.
- [43] Y. Han, S. Jin, C.-K. Wen, and T. Q. S. Quek, “Localization and channel reconstruction for extra large RIS-assisted massive MIMO systems,” *IEEE Journal of Selected Topics in Signal Processing*, vol. 16, no. 5, pp. 1011–1025, 2022.
- [44] M. Arulampalam, S. Maskell, N. Gordon, and T. Clapp, “A tutorial on particle filters for online nonlinear/non-gaussian bayesian tracking,” *IEEE Transactions on Signal Processing*, vol. 50, no. 2, pp. 174–188, 2002.
- [45] C. Ruan, Z. Zhang, H. Jiang, J. Dang, L. Wu, and H. Zhang, “Vector approximate message passing with sparse Bayesian learning for Gaussian mixture prior,” *China Communications*, vol. 20, no. 5, pp. 57–69, 2023.
- [46] X. Zhang, F. Labeau, L. Hao, and J. Liu, “Joint active user detection and channel estimation via Bayesian learning approaches in MTC communications,” *IEEE Transactions on Vehicular Technology*, vol. 70, no. 6, pp. 6222–6226, 2021.
- [47] Y. Liao, X. Li, and Z. Cai, “Machine learning based channel estimation for 5G NR-V2V communications: Sparse bayesian learning and Gaussian process regression,” *IEEE Transactions on Intelligent Transportation Systems*, vol. 24, no. 11, pp. 12 523–12 534, 2023.
- [48] A. Rajoriya, A. Kumar, and R. Budhiraja, “Covariance-free variational Bayesian learning for correlated block sparse signals,” *IEEE Communications Letters*, vol. 27, no. 3, pp. 966–970, 2023.
- [49] K. Keykhosravi, M. F. Keskin, G. Seco-Granados, P. Popovski, and H. Wymeersch, “RIS-enabled SISO localization under user mobility and spatial-wideband effects,” *IEEE Journal of Selected Topics in Signal Processing*, vol. 16, no. 5, pp. 1125–1140, 2022.
- [50] H. Wymeersch and B. Denis, “Beyond 5G wireless localization with reconfigurable intelligent surfaces,” in *ICC 2020 - 2020 IEEE International Conference on Communications (ICC)*, 2020, pp. 1–6.
- [51] G. Liu and X. Sun, “Two-stage matrix differencing algorithm for mixed far-field and near-field sources classification and localization,” *IEEE Sensors Journal*, vol. 14, no. 6, pp. 1957–1965, 2014.
- [52] Y. Lu, Z. Zhang, and L. Dai, “Hierarchical beam training for extremely large-scale MIMO: From far-field to near-field,” *IEEE Transactions on Communications*, pp. 1–1, 2023.
- [53] W.-C. Chang and Y. T. Su, “Sparse Bayesian learning based tensor dictionary learning and signal recovery with application to MIMO channel estimation,” *IEEE Journal of Selected Topics in Signal Processing*, vol. 15, no. 3, pp. 847–859, 2021.
- [54] C. W. Fox and S. J. Roberts, “A tutorial on variational Bayesian inference,” *Artificial intelligence review*, vol. 38, no. 2, pp. 85–95, 2012.
- [55] Y. Li, S. Ma, G. Yang, and K. Wong, “Robust localization for mixed LOS/NLOS environments with anchor uncertainties,” *IEEE Trans. Commun.*, vol. 68, no. 7, pp. 4507–4521, 2020.
- [56] F. Wen, P. Liu, H. Wei, Y. Zhang, and R. C. Qiu, “Joint azimuth, elevation, and delay estimation for 3-D indoor localization,” *IEEE Transactions on Vehicular Technology*, vol. 67, no. 5, pp. 4248–4261, 2018.
- [57] Y. Li, S. Ma, and G. Yang, “Robust localization with distance-dependent noise and sensor location uncertainty,” *IEEE Wireless Communications Letters*, vol. 10, no. 9, pp. 1876–1880, 2021.
- [58] Y. Shen and M. Z. Win, “Fundamental limits of wide-band localization— part I: A general framework,” *IEEE Transactions on Information Theory*, vol. 56, no. 10, pp. 4956–4980, 2010.